

Optimized high-order IMEX-RK schemes for degenerate diffusion-reaction problems with application to travelling waves phenomena*

Paola F. Antonietti [†]Mattia Corti [†]Giuseppe Orlando [‡]

Keywords: Degenerate diffusion-reaction problems, IMEX, polydG, travelling waves

Abstract

We study a class of IMPLICIT-EXPLICIT Runge–Kutta (IMEX-RK) schemes for the numerical approximation of reaction and diffusion-reaction problems arising in a variety of biological and physical applications. Such models may admit travelling wave solutions, with the Fisher–Kolmogorov equation representing a prototypical example. Motivated by this feature, the proposed time integration schemes are designed to accurately capture sharp propagating fronts. We also investigate a less standard use of IMEX-RK methods that circumvents a splitting of reaction terms into linear and nonlinear components, while still requiring the solution of linear systems at each stage. This semi-implicit formulation, referred to as SI-IMEX-RK, enables a targeted treatment of stiffness by isolating its relevant contributions. The time discretization is coupled with a high-order polygonal discontinuous Galerkin method for space discretization, resulting in a flexible and robust framework for the treatment of multiscale dynamics in complex geometries. A comprehensive validation strategy is presented to assess the accuracy and stability properties of the proposed schemes across a hierarchy of increasingly challenging test problems.

1 Introduction

Diffusion-reaction systems constitute a standard mathematical framework for modelling a wide range of phenomena arising, for instance, in ecology, combustion, and biology [31, 32, 36, 38, 64, 69]. A common numerical approach for approximating such systems is based on the method of lines. Within this framework, the spatial discretization of the governing equations is performed first, typically leading to a system of ordinary differential equations (ODEs) of the form

$$\frac{d\mathbf{y}}{dt} = \mathbf{F}_D(\mathbf{y}) + \mathbf{F}_R(\mathbf{y}, t),$$

***Fundings:** This work is partially funded by the European Union (ERC SyG, NEMESIS, project number 101115663). Views and opinions expressed are, however, those of the authors only and do not necessarily reflect those of the European Union or the European Research Council Executive Agency. Neither the European Union nor the granting authority can be held responsible for them. The present research is part of the activities of the Dipartimento di Eccellenza 2023-2027 grant, funded by MUR. MC acknowledges “INdAM - GNCS Project”, codice CUP E53C25002010001. PFA, MC, and GO are members of INdAM-GNCS.

[†]MOX-Dipartimento di Matematica, Politecnico di Milano, Piazza Leonardo da Vinci 32, Milan, 20133, Italy (paola.antonietti@polimi.it, mattia.corti@polimi.it)

[‡]CMAP, CNRS, École polytechnique, Institut Polytechnique de Paris, Route de Saclay, 91120 Palaiseau, France (giuseppe.orlando@polytechnique.edu)

where \mathbf{F}_D and \mathbf{F}_R denote the discrete diffusion and reaction operators, respectively. Several approaches have been proposed in the literature for the numerical solution of this problem, including exponential integrators [24], fully implicit schemes [65], operator splitting techniques [32, 36], and IMplicit-EXplicit (IMEX) Runge–Kutta (RK) methods [3, 31]. In this work, we focus on the latter class of methods. IMEX-RK methods have proven to be particularly effective for a wide range of multiscale problems, see, e.g., [17, 19, 20, 21, 35, 61, 62]. Our interest is specifically directed toward regimes in which the reaction term becomes dominant and therefore potentially stiff, making a fully explicit treatment prohibitively restrictive. In the singular limit, the differential system degenerates into an algebraic constraint, and IMEX-RK methods must satisfy additional order conditions [13, 14] to preserve the designed order of accuracy for the algebraic variable. At the same time, reaction operators are often (highly) nonlinear, so that a fully implicit discretization would require the solution of nonlinear systems at each time step or stage. Despite the absence of spatial coupling that allows decomposing the reaction term into independent local systems, such an approach may still be computationally inefficient. As far as the diffusion operator \mathbf{F}_D is concerned, we employ an implicit discretization. Nevertheless, we mention that stabilized explicit RK schemes based on Orthogonal Runge–Kutta–Chebyshev (ROCK) methods [1, 2] may represent an attractive alternative for the explicit treatment of diffusion-dominated problems. However, despite being formally explicit RK methods, ROCK schemes typically involve a very large number of stages, although they are designed to be low-storage and have a very low cost per stage. Moreover, ROCK methods are not naturally expressed in terms of classical Butcher tableaux, which makes their integration into standard RK frameworks less straightforward.

A commonly adopted strategy for problems involving nonlinear reaction terms consists in treating the linear part implicitly while discretizing the nonlinear contribution explicitly [25, 28]. This approach represents the first class of methods considered in this work. However, in order to avoid a rigid splitting between linear and nonlinear components of the reaction operator, we further develop a class of semi-implicit time discretizations based on IMEX Runge–Kutta schemes. Following the partitioned formulation proposed in [15], these methods — hereafter referred to as Semi-Implicit IMEX Runge–Kutta (SI-IMEX-RK) methods — allow one to identify and isolate the (possibly linear) source of stiffness within the system. As will be shown, this framework significantly enlarges the applicability of IMEX-RK methods and leads to efficient and flexible schemes that can be naturally extended to more complex nonlinear dependencies. Finally, we recall that diffusion-reaction systems may admit travelling wave solutions [6, 28, 40, 55]. Accurate numerical schemes for such problems should therefore provide a good approximation of the propagation speed and shape of these waves, while minimising artificial numerical dissipation and dispersion. This work tries to construct high-order IMEX-RK schemes that provide an improved numerical description of wave propagation properties. In this context, the main novelty of the proposed work lies in the development of schemes aimed at improving the numerical approximation of wave propagation and the algebraic accuracy. In addition, the SI-IMEX-RK framework is exploited to provide a more flexible treatment of stiff reaction mechanisms within the overall formulation.

The remainder of the paper is organized as follows. In Section 2, we introduce the mathematical model of interest together with the abstract system of ODEs considered throughout the paper. Section 3 is devoted to the time discretization strategy based on IMEX-RK methods. After recalling the properties of interest for the model under consideration, we first discuss a classical IMEX-RK approach based on an implicit treatment of the linear reaction term and an explicit discretization of the nonlinear contribution. We then introduce the novel SI-IMEX-RK methodology inspired

by [15]. In Section 4, we derive new high-order IMEX-RK schemes optimized with respect to the properties discussed in Section 3. In Section 5, we describe the chosen space discretization, which is based on a polytopal discontinuous Galerkin (polydG) method [26, 27]. Sections 6 and 7 present a collection of numerical experiments that validate the proposed methods on various ODEs and PDEs, respectively. Finally, conclusions and perspectives for future work are outlined in Section 8.

2 Mathematical model

In this section, we briefly outline the mathematical model. Let $\Omega \subset \mathbb{R}^d$, $d = 2, 3$, be a connected open bounded set with a sufficiently smooth boundary $\partial\Omega$ and denote by \mathbf{x} the spatial coordinates and by t the temporal coordinate. The boundary can be divided into two subsets Γ_D and Γ_N , where we impose Dirichlet and Neumann boundary conditions, respectively, and such that $\Gamma_D \cup \Gamma_N = \partial\Omega$ and $\Gamma_D \cap \Gamma_N = \emptyset$. We consider as model problem a possibly degenerate diffusion-reaction system with nonlinear reaction term: find $\mathbf{u} = \mathbf{u}(\mathbf{x}, t) \in \mathbb{R}^N$, with N denoting the number of components, such that

$$\frac{\partial \mathbf{u}}{\partial t} = \nabla \cdot (\boldsymbol{\Sigma} \nabla \mathbf{u}) + \mathbf{F}(\mathbf{u}, t), \quad \text{in } \Omega \times (0, T], \quad (2.1a)$$

$$\mathbf{u} = \mathbf{u}_D, \quad \text{on } \Gamma_D \times (0, T], \quad (2.1b)$$

$$\boldsymbol{\Sigma} \nabla \mathbf{u} \cdot \mathbf{n}_\Omega = \mathbf{g}_N, \quad \text{on } \Gamma_N \times (0, T], \quad (2.1c)$$

$$\mathbf{u}(\cdot, 0) = \mathbf{u}_0, \quad \text{in } \Omega, \quad (2.1d)$$

where $\boldsymbol{\Sigma} = \text{diag}(\sigma_1, \dots, \sigma_N)$ is the diagonal matrix containing the diffusion coefficients ($\sigma_j \geq 0$ for $j = 1, \dots, N$) and $\mathbf{F} : \mathbb{R}^N \rightarrow \mathbb{R}^N$ is the nonlinear reaction term. Moreover, $\mathbf{u}_D \in H^{1/2}(\Gamma_D)$ and $\mathbf{g}_N \in H^{-1/2}(\Gamma_N)$ are the Dirichlet and Neumann boundary conditions, respectively, while \mathbf{n}_Ω is the outward unit normal from the domain Ω . Finally, $\mathbf{u}_0 \in L^2(\Omega)$ is the initial condition. We denote by u_j the j -th component of the vectorial variable \mathbf{u} . As mentioned in the Introduction, a notable example of this class of problems is the Fisher–Kolmogorov (FK) equation [38], which will be introduced in Section 7.1 and will serve as relevant numerical testbed for validating our approach.

In the limit of dominant reaction, Equation (2.1) could be interpreted as a differential-algebraic equation (DAE), see, e.g., [13, 19]. Within the notation of (2.1), this corresponds to the presence of rapidly relaxing reaction dynamics that drive the solution toward a low-dimensional invariant manifold defined by $\mathbf{F}(\mathbf{u}, t) = \mathbf{0}$. More precisely, we assume that the system exhibits an *index-1* DAE structure, in the sense that the algebraic constraint $\mathbf{F}(\mathbf{u}, t) = \mathbf{0}$ defines locally a smooth manifold. In particular, we assume that the Jacobian matrix $\partial_{\mathbf{u}} \mathbf{F}(\mathbf{u}, t)$ is nonsingular when evaluated at the corresponding equilibrium solution, which guarantees that the constraint can be locally resolved with respect to \mathbf{u} by the implicit function theorem. This intrinsic stiffness and multiscale nature poses severe challenges for standard time integration methods, often leading to order reduction and loss of accuracy unless specifically designed strategies are employed. In particular, the coexistence of diffusive and (highly) stiff reactive dynamics calls for time discretizations that combine robustness, accuracy, and stability in a non-standard and non-trivial way, motivating the use of the time discretization strategies that will be depicted in Section 3. An additional structural feature of systems of the form (2.1) is that they may admit travelling wave solutions [6, 28, 29, 40], which play a fundamental role in the qualitative behaviour of the underlying dynamics. This observation motivates the development and investigation of novel time discretization schemes designed to improve the description of key wave propagation properties, as discussed in Sections 3 and 4.

3 Time discretization: IMEX-RK methods

In this work, we first focus on the time discretization of the governing problem (2.1). Regardless of the particular space discretization employed, the resulting semi-discrete problem can be written in the abstract form

$$\mathbf{M}\dot{\mathbf{U}}(t) + \mathbf{K}\mathbf{U}(t) = \mathbf{G}(\mathbf{U}(t), t), \quad t \in (0, T], \quad (3.1a)$$

$$\mathbf{U}(0) = \mathbf{U}_0. \quad (3.1b)$$

The specific form of the matrices, vectors, and discrete operators appearing in (3.1) depends on the chosen space discretization, and their expressions and interpretation will be detailed in Section 5. Since the time-integration procedure can be described independently of these space discretization details, we now discuss the temporal discretization of (3.1) by means of IMEX-RK methods [17, 49]. In particular, we recall some concepts related to IMEX-RK methods that will be particularly relevant in Section 4. IMEX-RK methods are represented compactly by the following two Butcher tableaux [22]

$$\begin{array}{c|c} \hat{\mathbf{c}} & \hat{\mathbf{A}} \\ \hline & \hat{\mathbf{b}}^\top \end{array} \quad \begin{array}{c|c} \mathbf{c} & \mathbf{A} \\ \hline & \mathbf{b}^\top \end{array}$$

with $\hat{\mathbf{A}} = \{\hat{a}_{lm}\}_{l,m=1,\dots,s}$, $\hat{\mathbf{b}} = \{\hat{b}_l\}_{l=1,\dots,s}$, and $\hat{\mathbf{c}} = \{\hat{c}_l\}_{l=1,\dots,s}$ denoting the explicit companion method of the IMEX-RK method, and $\mathbf{A} = \{a_{lm}\}_{l,m=1,\dots,s}$, $\mathbf{b} = \{b_l\}_{l=1,\dots,s}$, $\mathbf{c} = \{c_l\}_{l=1,\dots,s}$ denoting the implicit one. Here s denotes the number of stages of both explicit and implicit methods. Hence, an IMEX-RK method can be interpreted as the combination of two RK methods for which the coefficients \hat{a}_{lm} , a_{lm} , \hat{c}_l , c_l , \hat{b}_l , and b_l are determined so that the method is consistent of a given order. A detailed discussion on the coupling conditions for high-order IMEX-RK methods can be found in [62]. In particular, the following relation has to be satisfied [49]

$$\sum_{l=1}^s b_l = \sum_{l=1}^s \hat{b}_l = 1.$$

Moreover, the classical relations of RK methods for the quadrature nodes \mathbf{c} and $\hat{\mathbf{c}}$ [22, 50], i.e.

$$\sum_{m=1}^s a_{lm} = c_l, \quad \sum_{m=1}^s \hat{a}_{lm} = \hat{c}_l, \quad l = 1, \dots, s, \quad (3.2)$$

are assumed.

Definition 3.1 (IMEX-RK methods of type I/II/ARS [17]). *An IMEX-RK method is said to be of **type I** [62] if the matrix \mathbf{A} is invertible. It is said to be of **type II** [49] if the matrix \mathbf{A} can be written in the form*

$$\mathbf{A} = \begin{pmatrix} 0 & 0 \\ \mathbf{a} & \mathcal{A} \end{pmatrix},$$

with $\mathbf{a} = (a_{21}, \dots, a_{s1})^\top \in \mathbb{R}^{s-1}$ and the matrix $\mathcal{A} \in \mathbb{R}^{(s-1) \times (s-1)}$ is invertible. In the special case $\mathbf{a} = \mathbf{0}$, $b_1 = 0$, the method is said of **type ARS** (see [11]) and it is reducible to a method using $s - 1$ stages.

The formal accuracy imposed by the order conditions is typically not preserved in the case of very stiff problems [16, 45, 62] and one can incur in the so-called order reduction phenomenon [12, 45]. Hence, other properties have to be imposed to IMEX-RK methods so as to preserve full accuracy in a very stiff regime.

Definition 3.2 (Implicitly and global stiffly accurate methods [16]). *An IMEX-RK method is said to be **Implicitly Stiffly Accurate** or simply **Stiffly Accurate (SA)** if the implicit companion method is stiffly accurate, i.e. $a_{si} = b_i, i = 1, \dots, s$. An IMEX-RK method is said **Globally Stiffly Accurate** if it is Implicitly Stiffly Accurate and, in addition, the explicit companion method is First Same As Last, i.e. $\hat{a}_{si} = \hat{b}_i, i = 1, \dots, s$.*

Next, we recall some relevant properties that a time discretization method should obey for the problem of interest and their extension to IMEX-RK methods. The minimal requirement for the implicit method is to be A-stable. A RK method with a Butcher tableau given by $(\mathbf{A}, \mathbf{b}, \mathbf{c})$ is called A-stable if $|R(z)| \leq 1$ for $\text{Re}(z) \leq 0$ [50], where $R(z)$ is the stability function

$$R(z) = 1 + z\mathbf{b}^\top (\mathbf{I} - z\mathbf{A})^{-1} \mathbf{e},$$

with $\mathbf{e} = (1, 1, \dots, 1) \in \mathbb{R}^s$. The asymptotic properties of IMEX-RK methods are strongly related to the L-stability of the implicit part of the scheme. An implicit Runge–Kutta scheme is said to be L-stable [45] if it is A-stable and $R(z) \rightarrow 0$ as $z \rightarrow \infty$. Since the seminal work of [62], the use of L-stable methods in stiff nonlinear regimes has been widely regarded as the appropriate choice, as it endows the resulting scheme with intrinsic robustness against high-frequency disturbances that may arise. An L-stable method typically results from the combination of an A-stable method with a SA method [45]. However, for methods of type II where \mathbf{A} is not invertible, this combination does not necessarily lead to an L-stable method [19]. Then, the following supplementary condition is required to obtain the L-stability [19], i.e.

$$\mathbf{e}_s^\top \mathcal{A}^{-1} \mathbf{a} = \sum_{m=2}^s w_{sm} a_{m1} = 0, \quad (3.3)$$

where $\mathbf{e}_s^\top = (0, \dots, 0, 1)^\top$ and w_{lm} denotes the elements of the inverse of \mathcal{A} . In addition, L-stability alone is not sufficient to guarantee the desired order of accuracy when the method is applied to algebraic systems. In this case, supplementary conditions must be satisfied. Specifically, for type II schemes, one has to impose [19, 51]

$$\sum_{m=2}^s b_l w_{lm} w_{m2} = 0, \quad l = 2, \dots, s, \quad (3.4)$$

so as to ensure at least second-order accuracy for algebraic systems. For SA schemes, this condition reduces to $w_{s2} = 0$.

Another relevant property is related to the so-called *stage order*, i.e., the order of accuracy of each internal stage. As discussed in [52], the stage order is the minimum order of accuracy when a scheme is applied to stiff problems. It is defined as the maximum \hat{p} for which the following condition holds [13]

$$\sum_{m=1}^s a_{lm} c_m^{k-1} = \frac{1}{k} c_l^k, \quad 1 \leq k \leq \hat{p} \text{ and for all } l. \quad (3.5)$$

Numerical dissipation and dispersion

In this section, we recall several concepts related to dissipation and dispersion in the context of IMEX-RK methods. When dealing with wave phenomena, especially highly oscillatory and travelling waves, it is crucial to ensure low numerical dissipation in order to accurately capture wave amplitudes and low numerical dispersion to correctly reproduce phase speed and front propagation. A phase-lag analysis of RK methods is typically based on linear ODEs with oscillatory solutions (pure imaginary eigenvalues). More specifically, one considers the following test equation [39, 68]

$$\frac{dY}{dt} = i\omega Y + \delta \exp(i\omega_p t),$$

where i denotes the imaginary unit, whereas the natural frequency ω , the forcing frequency $\omega_p \neq \omega$, and the forcing amplitude δ are real numbers. To characterize dissipation properties, let $R(z) = P(z)/Q(z)$ and define the E -polynomial [59]

$$E(y) = |Q(iy)|^2 - |P(iy)|^2, \quad y \in \mathbb{R}. \quad (3.6)$$

Definition 3.3. A Runge–Kutta method is said to be dispersive of order q (q even) if $\phi(\omega\Delta t) = \omega\Delta t - \arg[R(i\omega\Delta t)] = \mathcal{O}\left((\omega\Delta t)^{q+1}\right)$, with $\Delta t > 0$ denoting the time step, or if, equivalently,

$$\sum_{i=0}^j \frac{(-1)^i r_i}{(j-1)!} = 0, \quad j = 1, 3, \dots, q-1,$$

where r_i are the coefficients of the Taylor expansion of $R(z)$, i.e. $R(z) = \sum_{i=0}^{\infty} r_i z^i$. A Runge–Kutta method is said to be dissipative of order r (r odd) if $d(\omega\Delta t) = 1 - |R(i\omega\Delta t)| = \mathcal{O}\left((\omega\Delta t)^{r+1}\right)$, or if, equivalently, $E_{2j} = 0$ for $0 \leq j \leq \frac{1}{2}(r-1)$, where E_{2j} denotes the coefficients of the E -polynomial (3.6).

3.1 IMEX-RK time discretization for diffusion-reaction PDEs

We are now in a position to introduce the semi-discrete IMEX-RK time discretization for problem (3.1). IMEX-RK methods are widely employed for time-dependent problems that can be decomposed into the sum of a stiff and a non-stiff component. Alternatively, they are commonly formulated by splitting the right-hand side of the resulting ODE into a linear term, treated implicitly, and a nonlinear term, discretized explicitly [25, 28]. In either formulation, such IMEX-RK methods are constructed in an *additive* fashion and therefore fall within the broader class of additive RK schemes [49].

Consider therefore the time-dependent problem $\frac{d\mathbf{y}}{dt} = \mathbf{f}_I(\mathbf{y}, t) + \mathbf{f}_E(\mathbf{y}, t)$, where I and E subscripts denote the components of the system discretized implicitly and explicitly, respectively. If $\mathbf{v}^n \approx \mathbf{y}(t^n)$, the generic l -stage IMEX-RK method reads as

$$\begin{aligned} \mathbf{v}^{(n,l)} = \mathbf{v}^n + \Delta t \sum_{m=1}^{l-1} \left[\hat{a}_{lm} \mathbf{f}_E \left(\mathbf{v}^{(n,m)}, t + \hat{c}_m \Delta t \right) + a_{lm} \mathbf{f}_I \left(\mathbf{v}^{(n,m)}, t + c_m \Delta t \right) \right] \\ + \Delta t \sum_{m=l}^s a_{lm} \mathbf{f}_I \left(\mathbf{v}^{(n,m)}, t + c_m \Delta t \right), \quad n \geq 0, \end{aligned} \quad (3.7)$$

where $l = 1, \dots, s$. After the computation of the intermediate stages, the final update \mathbf{v}^{n+1} is computed as

$$\mathbf{v}^{n+1} = \mathbf{v}^n + \Delta t \sum_{l=1}^s \left[\hat{b}_l \mathbf{f}_E \left(\mathbf{v}^{(n,l)}, t + \hat{c}_l \Delta t \right) + b_l \mathbf{f}_I \left(\mathbf{v}^{(n,l)}, t + c_l \Delta t \right) \right]. \quad (3.8)$$

We now apply (3.7)-(3.8) to (2.1a), then assuming therefore that $\mathbf{F}(\mathbf{u}, t) = \mathbf{F}_E(\mathbf{u}, t) + \mathbf{F}_I(\mathbf{u}, t)$, it yields the following expression for the generic l -stage

$$\begin{aligned} \mathbf{u}^{(n,l)} &= \mathbf{u}^n + \Delta t \sum_{m=1}^s a_{lm} \nabla \cdot \left(\Sigma \nabla \mathbf{u}^{(n,m)} \right) + \Delta t \sum_{m=l}^s a_{lm} \mathbf{F}_I \left(\mathbf{u}^{(n,m)}, t + c_m \Delta t \right) \\ &\quad + \Delta t \sum_{m=1}^{l-1} \left[\hat{a}_{lm} \mathbf{F}_E \left(\mathbf{u}^{(n,m)}, t + \hat{c}_m \Delta t \right) + a_{lm} \mathbf{F}_I \left(\mathbf{u}^{(n,m)}, t + c_m \Delta t \right) \right], \end{aligned} \quad (3.9)$$

whereas the final update reads

$$\mathbf{u}^{n+1} = \mathbf{u}^n + \Delta t \sum_{l=1}^s \left[b_l \nabla \cdot \left(\Sigma \nabla \mathbf{u}^{(n,l)} \right) + \hat{b}_l \mathbf{F}_E \left(\mathbf{u}^{(n,l)}, t + \hat{c}_l \Delta t \right) + b_l \mathbf{F}_I \left(\mathbf{u}^{(n,l)}, t + c_l \Delta t \right) \right]. \quad (3.10)$$

We observe that the diffusion term is treated implicitly. Throughout this work, we assume that the diffusion coefficients σ_j are constant or, at least, independent of \mathbf{u} . We will briefly further comment on this later in the manuscript.

Remark 3.1 (Application of IMEX-RK to Equation (3.1a)). *By applying the relations (3.9)-(3.10) to Equation (3.1a), the fully discrete generic l -stage reads*

$$\begin{aligned} \mathbf{U}^{(n,l)} &= \mathbf{U}^n - \mathbf{M}^{-1} \Delta t \sum_{m=1}^s a_{lm} \mathbf{K} \mathbf{U}^{(n,m)} + \mathbf{M}^{-1} \Delta t \sum_{m=l}^s a_{lm} \mathbf{G}_I \left(\mathbf{U}^{(n,m)}, t + c_m \Delta t \right) \\ &\quad + \mathbf{M}^{-1} \Delta t \sum_{m=1}^{l-1} \left[\hat{a}_{lm} \mathbf{G}_E \left(\mathbf{U}^{(n,m)}, t + \hat{c}_m \Delta t \right) + a_{lm} \mathbf{G}_I \left(\mathbf{U}^{(n,m)}, t + c_m \Delta t \right) \right], \end{aligned} \quad (3.11)$$

whereas the final update reads

$$\begin{aligned} \mathbf{U}^{n+1} &= \mathbf{U}^n - \mathbf{M}^{-1} \Delta t \sum_{l=1}^s b_l \mathbf{K} \mathbf{U}^{(n,l)} \\ &\quad + \mathbf{M}^{-1} \Delta t \sum_{l=1}^s \left[\hat{b}_l \mathbf{G}_E \left(\mathbf{U}^{(n,l)}, t + \hat{c}_l \Delta t \right) + b_l \mathbf{G}_I \left(\mathbf{U}^{(n,l)}, t + c_l \Delta t \right) \right]. \end{aligned} \quad (3.12)$$

Here \mathbf{U} denotes the vector of the degrees of freedom, whereas \mathbf{G}_E and \mathbf{G}_I denote the spatial approximation of \mathbf{F}_E and \mathbf{F}_I , respectively.

3.2 SI-IMEX-RK time discretization for diffusion-reaction PDEs

Additive RK methods are commonly adopted for systems admitting a decomposition into the sum of stiff and non-stiff terms. However, the stiff dependence can be (highly) nonlinear, thus requiring

the solution of a nonlinear system at each stage. In other cases, the stiffness may be associated only to some variables [15]. Let us consider a *partitioned* time-dependent system

$$\frac{d\mathbf{y}_E}{dt} = \mathbf{f}_E(\mathbf{y}_E, \mathbf{y}_I, t), \quad (3.13a)$$

$$\frac{d\mathbf{y}_I}{dt} = \frac{1}{\varepsilon} \mathbf{f}_I(\mathbf{y}_E, \mathbf{y}_I, t), \quad (3.13b)$$

where \mathbf{y}_E and \mathbf{y}_I may be vectors of different dimensions and $\mathbf{y}_E(0) = \mathbf{y}_{E,0}, \mathbf{y}_I(0) = \mathbf{y}_{I,0}$ are the initial conditions. The stiffness of the system is associated to the variables \mathbf{y}_I under the assumption $0 < \varepsilon \ll 1$.

We now introduce a class of Semi-Implicit IMEX-RK (SI-IMEX-RK) methods for problem (2.1), in a sense that will be made precise below. Following the approach proposed in [15], we rewrite (2.1a) as the following partitioned system

$$\frac{\partial \mathbf{u}_E}{\partial t} = \nabla \cdot (\boldsymbol{\Sigma} \nabla \mathbf{u}_I) + \mathbf{F}(\mathbf{u}_E, \mathbf{u}_I, t), \quad (3.14a)$$

$$\frac{\partial \mathbf{u}_I}{\partial t} = \nabla \cdot (\boldsymbol{\Sigma} \nabla \mathbf{u}_I) + \mathbf{F}(\mathbf{u}_E, \mathbf{u}_I, t), \quad (3.14b)$$

with initial conditions $\mathbf{u}_E = \mathbf{u}_0, \mathbf{u}_I = \mathbf{u}_0$ and supplied with compatible boundary conditions. Subscripts E and I in (3.14) indicate the explicit and (semi-)implicit treatment of the first and the second term of \mathbf{F} , respectively. In this setting, the solution of (3.14) satisfies $\mathbf{u}_E = \mathbf{u}_I$ for any $t \geq 0$ and is also a solution of (2.1).

The SI-IMEX-RK framework is obtained by applying a partitioned IMEX Runge–Kutta method to system (3.14). For simplicity, and following [15], we assume that the system is autonomous, i.e. $\mathbf{F}(\mathbf{u}_E, \mathbf{u}_I, t) = \mathbf{F}(\mathbf{u}_E, \mathbf{u}_I)$. Extensions to non-autonomous problems, as well as to the case $\mathbf{c} \neq \widehat{\mathbf{c}}$, would unnecessarily complicate the presentation of the core ideas; we refer to [15] for a detailed discussion. A crucial assumption is instead that the weights of the implicit and explicit tableaux coincide, i.e. $\mathbf{b}^\top = \widehat{\mathbf{b}}^\top$. The relevance of this condition will become clear shortly. However, we emphasize that this requirement is important independently of the SI-IMEX-RK construction, as it is necessary to ensure the preservation of linear invariants [43]. Under these assumptions, the generic l -stage of the SI-IMEX-RK method applied to (2.1) reads as in Algorithm 1.

Owing to the condition $\mathbf{b}^\top = \widehat{\mathbf{b}}^\top$, we obtain $\mathbf{u}_E^{n+1} = \mathbf{u}_I^{n+1} = \mathbf{u}^{n+1}$ for all n , showing that the duplication of variables is purely formal.

The main advantage of this approach lies in the identification of a suitable (possibly linear) implicit dependence, which avoids the solution of (highly) nonlinear systems or the need for stage-by-stage linearization. Moreover, in the presence of nonlinear diffusion, e.g., $\boldsymbol{\Sigma} = \boldsymbol{\Sigma}(\mathbf{u})$, the same framework can be naturally extended by evaluating the diffusion coefficient explicitly as $\boldsymbol{\Sigma}(\mathbf{u}_E)$, thereby retaining a fully linear implicit solve at each stage.

Remark 3.2 (Application of IMEX-RK to Equation (3.1a)). *The l -stage of the SI-IMEX-RK method in Algorithm 1 for problem (3.1a) reads*

$$\mathbf{U}_E^{(n,l)} = \mathbf{U}^n - \mathbf{M}^{-1} \Delta t \sum_{m=1}^{l-1} \hat{a}_{lm} \mathbf{K} \mathbf{U}_I^{(n,m)} + \mathbf{M}^{-1} \Delta t \sum_{m=1}^{l-1} \hat{a}_{lm} \mathbf{G} \left(\mathbf{U}_E^{(n,m)}, \mathbf{U}_I^{(n,m)} \right), \quad (3.18a)$$

$$\mathbf{U}_I^{(n,l)} = \mathbf{U}^n - \mathbf{M}^{-1} \Delta t \sum_{m=1}^s a_{lm} \mathbf{K} \mathbf{U}_I^{(n,m)} + \mathbf{M}^{-1} \Delta t \sum_{m=1}^s a_{lm} \mathbf{G} \left(\mathbf{U}_E^{(n,m)}, \mathbf{U}_I^{(n,m)} \right), \quad (3.18b)$$

Algorithm 1 SI-IMEX-RK scheme for (2.1)

Input: $\mathbf{u}^0 = \mathbf{u}_0$, final time T , time step Δt , Butcher tableaux $(a_{lm}, \hat{a}_{lm}, b_l)$
for $l = 1, \dots, s$ **do**

Step 1 (explicit stage). Compute

$$\mathbf{u}_E^{(n,l)} = \mathbf{u}^n + \Delta t \sum_{m=1}^{l-1} \hat{a}_{lm} \nabla \cdot \left(\boldsymbol{\Sigma} \nabla \mathbf{u}_I^{(n,m)} \right) + \Delta t \sum_{m=1}^{l-1} \hat{a}_{lm} \mathbf{F} \left(\mathbf{u}_E^{(n,m)}, \mathbf{u}_I^{(n,m)} \right). \quad (3.15)$$

Step 2 (implicit stage). Solve for $\mathbf{u}_I^{(n,l)}$:

$$\begin{aligned} \mathbf{u}_I^{(n,l)} - \Delta t a_{ll} \nabla \cdot \left(\boldsymbol{\Sigma} \nabla \mathbf{u}_I^{(n,l)} \right) &= \mathbf{u}^n \\ &+ \Delta t \sum_{m=1}^{l-1} a_{lm} \nabla \cdot \left(\boldsymbol{\Sigma} \nabla \mathbf{u}_I^{(n,m)} \right) + \Delta t \sum_{m=1}^l a_{lm} \mathbf{F} \left(\mathbf{u}_E^{(n,m)}, \mathbf{u}_I^{(n,m)} \right). \end{aligned} \quad (3.16)$$

end for

Step 3 (update). Set

$$\mathbf{u}^{n+1} = \mathbf{u}^n + \Delta t \sum_{l=1}^s b_l \nabla \cdot \left(\boldsymbol{\Sigma} \nabla \mathbf{u}_I^{(n,l)} \right) + \Delta t \sum_{l=1}^s b_l \mathbf{F} \left(\mathbf{u}_E^{(n,l)}, \mathbf{u}_I^{(n,l)} \right). \quad (3.17)$$

whereas the final update reads

$$\mathbf{U}^{n+1} = \mathbf{U}^n - \mathbf{M}^{-1} \Delta t \sum_{l=1}^s b_l \mathbf{K} \mathbf{U}_I^{(n,l)} + \mathbf{M}^{-1} \Delta t \sum_{l=1}^s b_l \mathbf{G} \left(\mathbf{U}_E^{(n,m)}, \mathbf{U}_I^{(n,m)} \right). \quad (3.19)$$

Here \mathbf{U}_E and \mathbf{U}_I denote the vectors of the degrees of freedom for the explicit and (semi)-implicit components, respectively.

4 Optimized IMEX-RK for degenerate diffusion-reaction PDEs

In this section, we propose third and fourth-order IMEX-RK schemes that optimize the properties discussed in Section 3 and are therefore particularly well suited for model (2.1). The symbolic computations have been carried out using both `MATLAB` and `sympy` [57] in combination with `ponio` [33, 56] for the symbolic derivation of the stability functions. For the novel schemes derived in this work, we adopt the notation IMEX(p, s)-X, where p denotes the order of the method, and s represents the number of stages of both the implicit and explicit schemes. The symbol X denotes a key distinguishing property of the method. As will become clear in the following, all the proposed methods achieve stage order 2, and their implicit part is always L-stable. Since these two features constitute essential requirements in the derivation, we do not include them in the nomenclature in order to keep it concise.

First, we assume that the implicit scheme is a Explicit Singly Diagonally Implicit Runge–Kutta (ESDIRK) method, namely \mathbf{A} is lower triangular, $a_{ll} = \gamma > 0$ with $l = 2, \dots, s$, and the first row is zero. Hence, the first stage is only formal, unless necessary to achieve stage order 2

(see relation (3.5)). Finally, to guarantee full accuracy in the stiff regime, we consider a L-stable method, as discussed in Section 3. A similar analysis for ESDIRK schemes has been conducted in [54]. Then, starting from the implicit method, an explicit companion method is obtained in order to satisfy the order and coupling conditions [62].

Several alternative IMEX strategies have been proposed in the literature for diffusion-reaction problems, (i.e., [3, 47, 48]). In particular, we mention the PIROCK method [3], where second-order SDIRK schemes are coupled with explicit second-order ROCK integrators [1, 2], facilitating the inclusion of non-trivial, possibly nonlinear operators. However, extending PIROCK to higher order is not straightforward. The semi-implicit approach in Section 3.2 provides an alternative strategy.

4.1 Third-order IMEX-RK schemes

In this section, we derive some third-order time discretization schemes that satisfy the largest possible number of the properties described in Section 3. All the derived schemes are assumed to be L-stable and of stage order 2 in their implicit part. Moreover, we impose the supplementary condition (3.4), together with high-order dissipation or dispersion requirements and additional order conditions for improved accuracy when solving algebraic systems. We recall that the considered IMEX-RK schemes satisfy condition (3.2). The conditions to achieve third-order accuracy for a RK method $(\mathbf{A}, \mathbf{b}, \mathbf{c})$ read as follows

$$\sum_{l=1}^s b_l = 1, \quad \sum_{l=1}^s b_l c_l = \frac{1}{2}, \quad (4.1a)$$

$$\sum_{l=1}^s b_l c_l^2 = \frac{1}{3}, \quad \sum_{l,m=1}^s b_l a_{lm} c_m = \frac{1}{6}. \quad (4.1b)$$

The coupling conditions to obtain a third order IMEX-RK method are

$$\begin{aligned} \sum_{l=1}^s b_l \hat{c}_l &= \frac{1}{2}, & \sum_{l=1}^s \hat{b}_l c_l &= \frac{1}{2}, & \sum_{l=1}^s \hat{b}_l \hat{c}_l^2 &= \frac{1}{3}, & \sum_{l=1}^s \hat{b}_l \hat{c}_l c_l &= \frac{1}{3}, \\ \sum_{l=1}^s b_l \hat{c}_l^2 &= \frac{1}{3}, & \sum_{l=1}^s b_l \hat{c}_l c_l &= \frac{1}{3}, & \sum_{l,m=1}^s b_l \hat{a}_{lm} c_m &= \frac{1}{6}, & \sum_{l,m=1}^s b_l a_{lm} \hat{c}_m &= \frac{1}{6}, \\ \sum_{l,m=1}^s b_l \hat{a}_{lm} \hat{c}_m &= \frac{1}{6}, & \sum_{l,m=1}^s \hat{b}_l \hat{a}_{lm} c_m &= \frac{1}{6}, & \sum_{l,m=1}^s \hat{b}_l a_{lm} \hat{c}_m &= \frac{1}{6}, & \sum_{l,m=1}^s \hat{b}_l a_{lm} c_m &= \frac{1}{6}. \end{aligned}$$

One can easily notice that 12 coupling conditions are necessary in the general case $\mathbf{b}^\top \neq \hat{\mathbf{b}}^\top, \mathbf{c} \neq \hat{\mathbf{c}}$ which reduce to 3 coupling conditions if $\mathbf{b}^\top = \hat{\mathbf{b}}^\top$ or to 2 coupling condition if $\mathbf{c} = \hat{\mathbf{c}}$. If both $\mathbf{b}^\top = \hat{\mathbf{b}}^\top$ and $\mathbf{c} = \hat{\mathbf{c}}$, zero coupling conditions are necessary. Finally, the additional order conditions up to third order that guarantee better accuracy for an algebraic system are [19]

$$\sum_{l,m=2}^s b_l w_{lm} \hat{c}_m = 1, \quad \sum_{l,m=2}^s b_l w_{lm} \hat{c}_m^2 = 1, \quad \sum_{l,m,k=2}^s b_l w_{lm} \hat{a}_{mk} \hat{c}_k = \frac{1}{2}, \quad (4.2)$$

where w_{lm} are the elements of the inverse of the matrix \mathcal{A} (see Definition 3.1).

Following the analysis in [14], we focus on five-stage ($s = 5$) IMEX-RK schemes, which represent the minimum number of stages required to simultaneously achieve L-stability and satisfy the

supplementary condition (3.4) [14]. Five-stage stiffly-accurate ESDIRK methods have 10 degrees of freedom (see Table 1).

0	0	0	0	0	0
c_2	$c_2 - \gamma$	γ	0	0	0
c_3	$c_3 - a_{32} - \gamma$	a_{32}	γ	0	0
c_4	$c_4 - a_{42} - a_{43} - \gamma$	a_{42}	a_{43}	γ	0
1	$1 - a_{52} - a_{53} - a_{54} - \gamma$	a_{52}	a_{53}	a_{54}	γ
	$1 - a_{52} - a_{53} - a_{54} - \gamma$	a_{52}	a_{53}	a_{54}	γ

Table 1: Butcher tableau of the implicit five-stage stiffly-accurate ESDIRK method.

The coefficients $c_2, a_{32}, a_{42}, a_{43}, a_{52}, a_{53}$, and a_{54} , together with the associated determining conditions, are reported in Table 2. For later use, we recall the E-polynomial (3.6), which, as reported

Coefficient	Condition used
$a_{52} = \frac{\frac{1}{2} - \gamma - a_{53}c_3 - a_{54}c_4}{c_2}$	Order conditions (4.1a)-(4.1b)
$a_{53} = \frac{\gamma(c_2 - 1) - a_{54}c_4(c_2 - c_4) + \frac{c_2}{2} - \frac{1}{3}}{c_3(c_2 - c_3)}$	Order conditions (4.1a)-(4.1b)
$a_{42} = \frac{\gamma^2 - \gamma - a_{32}a_{53}c_2 - a_{43}a_{54}c_3 + \frac{1}{6}}{a_{54}c_2}$	Order conditions (4.1a)-(4.1b)
$c_2 = 2\gamma$	Stage order 2 (3.5)
$a_{32} = \frac{c_3(c_3 - 2\gamma)}{4\gamma}$	Stage order 2 (3.5)
$a_{43} = \frac{\gamma(6\gamma^3 - 18\gamma^2 + 9\gamma - 1)}{3a_{54}c_3(2\gamma - c_3)}$	L-stability (3.3)
$a_{54} = \frac{\gamma(2\gamma - 1 + c_3(1 - \gamma))}{c_4(c_3 - c_4)}$	Supplementary algebraic condition (3.4)

Table 2: Expressions of the coefficients for the five-stage third-order implicit scheme obtained from order conditions, stage order 2, L-stability and supplementary algebraic condition (3.4).

in [19, 50], reduces to

$$\begin{aligned}
 E(y) = \gamma^8 y^8 + \left(-\frac{1}{36} + \frac{2}{3}\gamma - 6\gamma^2 + \frac{76}{3}\gamma^3 - 52\gamma^4 + 48\gamma^5 - 12\gamma^6 \right) y^6 \\
 + \left(\frac{1}{12} - \frac{4}{3}\gamma + 6\gamma^2 - 8\gamma^3 + 2\gamma^4 \right) y^4
 \end{aligned} \tag{4.3}$$

Then, the region of A-stability (hence L-stability) is given by the following interval [19, 45, 50]

$$0.2236478009341764510696898 \leq \gamma \leq 0.5728160624821348554080014. \tag{4.4}$$

Moreover, one can easily verify that the first two index-1 DAE accuracy conditions (4.2) are identically satisfied. We are left with 3 free parameters, i.e. c_3, c_4 , and γ . Several choices can be

considered to determine c_3 and c_4 . For instance, one may impose stage order 3 for the intermediate stages, or alternatively analyze the stability region of the internal stages, the so-called internal stability [50]. The investigation performed suggests that better results are obtained when stage order 3 is imposed on the third and fourth intermediate stages. Moreover, this choice preserves the high-order accuracy as much as possible, thereby avoiding degradation of the high-order accuracy of the spatial discretization (see Section 5). Finally, an alternative closure for c_3 will be discussed below when deriving the explicit method. Hence, imposing stage order 3 for the third intermediate stage leads to two admissible values for c_3

$$c_3 = c_3^{(1\pm)} = \gamma \left(3 \pm \sqrt{3} \right), \quad (4.5)$$

whereas imposing stage order 3 for the fourth (penultimate) intermediate stage yields two admissible values for c_4

$$c_4 = c_4^{(1\pm)} = \frac{-6\gamma^3 + 6\gamma^2(c_3 + 1) - 3\gamma(2c_3 + 1) \pm \sqrt{(6\gamma^2 - 2c_3(3\gamma - 1) - 1)(6\gamma^4 - 6\gamma^3(c_3 + 2) + 3\gamma^2(6c_3 - 1) + 2\gamma(3 - 7c_3) + 2c_3 - 1) + 1}}{2((c_3 - 2)(\gamma - 1) - 1)}. \quad (4.6)$$

Finally, we are left with one free parameter γ . In this work, we consider $\gamma = 0.435866521508482$ used also for the ARS(3,4,3) scheme in [11], the ARK3(2)4L[2]SA scheme in [49], and the MARS(3,4,3) and MARK3(2)4L[2]SA schemes in [13], as well as the BHR(5,5,3) in [14]. Whenever schemes are taken or adapted from the literature, we adopt the notation of the related reference where available. As an alternative, since as already mentioned (2.1a) may be characterized by a travelling-wave solution, we maximize the order of dissipation and dispersion. Regarding the order of dissipation, owing to Definition (3.3), we solve $E_4 = 0$ in (4.3) to obtain dissipation order 5. This gives $\gamma = 0.572816062482135$, which is the limit of the I-stability, hence L-stability (4.4). A slightly different value, namely $\gamma = 0.57281606248208$ has been considered in [19]. Regarding the order of dispersion, one can easily verify that

$$D(j) = \sum_{i=0}^j \frac{(-1)^i r_i}{(j-1)!} = 0, \quad \text{for } j = 1, 3,$$

where we recall that r_i are the coefficients of the Taylor expansion of $R(z)$ (see Definition (3.3)). Imposing $D(j) = 0$ for $j = 5$ so as to obtain an implicit RK-method with dispersion order equal to 6 leads to the following equation

$$4\gamma^5 - 16\gamma^4 + 14\gamma^3 - \frac{14}{3}\gamma^2 + \frac{2}{3}\gamma - \frac{1}{30} = 0.$$

The only solution that guarantees L-stability is $\gamma = 0.525721461435005$. Hence, if $\gamma = 0.525721461435005$ the implicit method has a dispersion order of 6, otherwise its dispersion order is 4.

Next, we consider an explicit companion method for the IMEX scheme. We consider $\hat{\mathbf{b}} = \mathbf{b}$ and $\hat{\mathbf{c}} = \mathbf{c}$, which results in 6 degrees of freedom. The corresponding Butcher tableau then reads as follows (Table 3)

0	0	0	0	0	0
c_2	c_2	0	0	0	0
c_3	$c_3 - \hat{a}_{32}$	\hat{a}_{32}	0	0	0
c_4	$c_4 - \hat{a}_{42} - \hat{a}_{43}$	\hat{a}_{42}	\hat{a}_{43}	0	0
1	$1 - \hat{a}_{52} - \hat{a}_{53} - \hat{a}_{54}$	\hat{a}_{52}	\hat{a}_{53}	\hat{a}_{54}	0
	$1 - a_{52} - a_{53} - a_{54} - \gamma$	a_{52}	a_{53}	a_{54}	γ

Table 3: Butcher tableau of the explicit five-stage method.

Since $\widehat{\mathbf{b}} = \mathbf{b}$ and $\widehat{\mathbf{c}} = \mathbf{c}$, no coupling condition with the implicit companion method is required to obtain a third order IMEX scheme (see the discussion in Section 3). However, we are left with the last condition in (4.1b) to ensure that the explicit method is of the third order, from which we get

$$\hat{a}_{52} = \frac{-\frac{\gamma\hat{a}_{54}c_4}{2} - \gamma(\hat{a}_{32}a_{53} + \hat{a}_{42}a_{54}) - \frac{c_3(\gamma\hat{a}_{53} + \hat{a}_{43}a_{54})}{2} + \frac{1}{12}}{\gamma^2}.$$

Next, we impose the condition (4.2) that guarantees third order accuracy for the algebraic variable, from which we obtain

$$\hat{a}_{43} = \frac{1 - 3\gamma(4\hat{a}_{32}a_{53} + 4\hat{a}_{42}a_{54} + 1)}{6a_{54}c_3}.$$

Moreover, one can easily verify that this condition is equivalent to imposing stage order 2 for the fifth (last) intermediate stage. Imposing stage order 2 for the third stage yields

$$\hat{a}_{32} = \hat{a}_{32}^{(1)} = \frac{c_3^2}{2c_2}, \quad (4.7)$$

while imposing stage order 2 for the fourth intermediate stage reduces to

$$\hat{a}_{32} = \hat{a}_{32}^{(2)} = \frac{1 - 3\gamma - 3b_4c_4^2}{12\gamma b_3}. \quad (4.8)$$

The only admissible solution which guarantees that both (4.7) and (4.8) are satisfied is $a_{52} = 0$ [19, 51], i.e.

$$c_3 = c_3^{(2)} = \frac{2(6\gamma^2 - 6\gamma + 1)}{3(2\gamma^2 - 4\gamma + 1)}. \quad (4.9)$$

If such condition is not imposed, then it is possible to fix the stage order 2 only for one of the two intermediate stages, and in such case, we consider $\hat{a}_{32}^{(1)}$.

We are now left with three free parameters, i.e. \hat{a}_{42} , \hat{a}_{53} , and \hat{a}_{54} . Following [19], we fix \hat{a}_{53} such that

$$\sum_{l,m,k} b_l \hat{a}_{lm} \hat{a}_{mk} c_k = \frac{1}{24},$$

so as to obtain the stability region of a fourth order explicit method. Hence, we get

$$\hat{a}_{53} = \frac{\gamma\hat{a}_{54}(\gamma + b_3c_3^2 - \frac{1}{3}) + \frac{1}{12}a_{54}(24\gamma\hat{a}_{42}a_{54}c_3 + 2c_3(3\gamma + 3a_{53}c_3^2 - 1) + 1)}{\gamma a_{54}c_3^2}.$$

The coefficient \hat{a}_{54} is determined by analyzing the E-polynomial associated to the Butcher tableau 3 so as to enhance the order of dissipation. After some tedious calculations, one can show that $E_4 = 0$ and that

$$E_6 = \frac{\gamma\hat{a}_{54}c_3(144\gamma\hat{a}_{42}a_{54} + 36\gamma + 36a_{53}c_3^2 - 12) + b_4}{72b_4}$$

so that, imposing $E_6 = 0$ in order to achieve dissipation order 7 (see Definition 3.3), we obtain

$$\hat{a}_{54} = \hat{a}_{54}^{(1)} = -\frac{b_4}{12\gamma c_3(12\gamma\hat{a}_{42}a_{54} + 3\gamma + 3a_{53}c_3^2 - 1)}. \quad (4.10)$$

If one instead desires dispersion order 6, which is the maximum attainable [68], calculations analogous to those described for the implicit scheme show that

$$\hat{a}_{54} = \hat{a}_{54}^{(2)} = -\frac{b_4}{10\gamma c_3 (12\gamma \hat{a}_{42} a_{54} + 3\gamma + 3a_{53} c_3^2 - 1)}. \quad (4.11)$$

Finally, the remaining parameter \hat{a}_{42} may be determined by imposing stage order 3 for the fourth (penultimate) intermediate stage. However, following [19], we consider the choice $\hat{a}_{42} = 0$, which our investigation shows to yield better results and will therefore be adopted in the following. In conclusion, following the nomenclature introduced at the beginning of Section 4, the third-order schemes derived in this work will be denoted by IMEX(3, 5)-LDs when $\hat{a}_{54}^{(1)}$ is employed, highlighting the Low Dissipation (LDs) of the explicit part, and by IMEX(3, 5)-LDp when $\hat{a}_{54}^{(2)}$ is used, highlighting the Low Dispersion (LDp) of the explicit part. A subscript will be used to distinguish between the (sub-)variants. We emphasize that all the schemes are characterized by low dispersion in the implicit part. The coefficients can be found in Appendix A (Tables 12-14).

4.2 Fourth-order IMEX-RK schemes

In this section, we consider fourth-order time discretization schemes. The conditions to achieve fourth-order accuracy for a Runge–Kutta method $(\mathbf{A}, \mathbf{b}, \mathbf{c})$ read as follows

$$\sum_{l=1}^s b_l = 1, \quad \sum_{l=1}^s b_l c_l = \frac{1}{2}, \quad \sum_{l=1}^s b_l c_l^2 = \frac{1}{3}, \quad \sum_{l,m=1}^s b_l a_{lm} c_m = \frac{1}{6}, \quad (4.12a)$$

$$\sum_{l=1}^s b_l c_l^3 = \frac{1}{4}, \quad \sum_{l,m=1}^s b_l c_l a_{lm} c_m = \frac{1}{8}, \quad \sum_{l,m=1}^s b_l a_{lm} c_m^2 = \frac{1}{12}, \quad \sum_{l,m,k=1}^s b_l a_{lm} a_{mk} c_k = \frac{1}{24}. \quad (4.12b)$$

In the general case $\mathbf{b}^\top \neq \hat{\mathbf{b}}^\top, \mathbf{c} \neq \hat{\mathbf{c}}$, 56 coupling conditions are necessary to obtain a fourth order accurate IMEX-RK method [62]. The coupling conditions reduce to 21 if $\mathbf{b}^\top = \hat{\mathbf{b}}^\top$ or to 12 if $\mathbf{c} = \hat{\mathbf{c}}$ [62]. We consider $\mathbf{b}^\top = \hat{\mathbf{b}}^\top$ and $\mathbf{c} = \hat{\mathbf{c}}$, so that only 2 coupling conditions are necessary [37], i.e.

$$\sum_{l,m,k=1}^s b_l a_{lm} \hat{a}_{mk} c_k = \frac{1}{24}, \quad \sum_{l,m,k=1}^s b_l \hat{a}_{lm} a_{mk} c_k = \frac{1}{24}. \quad (4.13)$$

Finally, the additional order conditions up to fourth order that guarantee better accuracy for an index-1 DAE can be obtained by imposing that the numerical solution and the exact solution agree up to a certain order in the Hilbert expansion with respect to the small parameter ε of (3.13b) [19]. Such order conditions can be also obtained with the help of the so-called bicolour rooted trees [14, 45]. Tedious calculations (see Appendix B) show that the supplementary order conditions for a fourth-order method are

$$\sum_{l,m=2}^s b_l w_{lm} \hat{c}_m = 1, \quad \sum_{l,m=2}^s b_l w_{lm} \hat{c}_m^2 = 1, \quad \sum_{l,m,k=2}^s b_l w_{lm} \hat{a}_{mk} \hat{c}_k = \frac{1}{2}, \quad (4.14a)$$

$$\sum_{l,m=2}^s b_l w_{lm} \hat{c}_m^3 = 1, \quad \sum_{l,m,k=2}^s b_l w_{lm} \hat{a}_{mk} \hat{c}_k^2 = \frac{1}{3}, \quad \sum_{l,m,k,j=2}^s b_l w_{lm} \hat{a}_{mk} \hat{a}_{kj} \hat{c}_j = \frac{1}{6}, \quad (4.14b)$$

$$\sum_{l,m,k=2}^s b_l w_{lm} \hat{c}_m \hat{a}_{mk} \hat{c}_k = \frac{1}{2}. \quad (4.14c)$$

We immediately consider six-stage ($s = 6$) fourth-order time discretization schemes. Indeed, as discussed, e.g., in [50], when considering a five-stage fourth-order time discretization scheme, L-stability is guaranteed only for a discrete set of values of γ . Hence, it is not possible to mimic the analysis performed in Section 4.1 in terms of optimizing the dispersion properties of the scheme. Six-stage stiffly-accurate ESDIRK methods have 16 degrees of freedom (Table 4)

0	0	0	0	0	0	0	0
c_2	$c_2 - \gamma$	γ	0	0	0	0	0
c_3	$c_3 - a_{32} - \gamma$	a_{32}	γ	0	0	0	0
c_4	$c_4 - a_{42} - a_{43} - \gamma$	a_{42}	a_{43}	γ	0	0	0
c_5	$c_5 - a_{51} - a_{52} - a_{53} - a_{54} - \gamma$	a_{51}	a_{52}	a_{53}	γ	0	0
1	$1 - a_{62} - a_{63} - a_{64} - a_{65} - \gamma$	a_{62}	a_{63}	a_{64}	a_{65}	γ	0
	$1 - a_{62} - a_{63} - a_{64} - a_{65} - \gamma$	a_{62}	a_{63}	a_{64}	a_{65}	γ	0

Table 4: Butcher tableau of the implicit six-stage stiffly-accurate ESDIRK method.

Considering the order conditions (4.12), stage order equal to 2, results in 7 remaining degrees of freedom which we identify in $a_{53}, a_{54}, b_5, c_3, c_4, c_5$, and γ . Unfortunately, the expressions of the remaining coefficients with respect to these free parameters are too complex to be obtained symbolically. Requiring the scheme is L-stable results allows to compute, e.g., a_{53} , and the following restriction on γ

$$0.247005962517487 \leq \gamma \leq 0.676042393226281. \quad (4.15)$$

Notice that, while the upper bound is identical to that reported in [50, 51], the lower bound is slightly different. Following, the analysis in Section 4.1, the value of γ is determined imposing order of dispersion equal to 6, and results in $\gamma = 0.2780538841136452$. Finally, another free parameter, e.g., a_{53} is determined imposing the algebraic condition (3.4). One can also verify that the supplementary conditions (4.14) that do not depend on the explicit companion method are satisfied. Hence, we are left with 4 free parameters, e.g., b_5, c_3, c_4, c_5 . Following [14, 51], b_5 is determined setting $b_2 = 0$. Several choices are possible for the remaining coefficients. We have analyzed both stage order and internal stability, and identified three schemes that exhibit superior overall accuracy (see Tables 18-20). We refer to the end of the section for a description of the properties of such schemes.

Now, we need to build an explicit companion method on top of it. Obviously, we consider $\mathbf{b} = \hat{\mathbf{b}}$ and $\mathbf{c} = \hat{\mathbf{c}}$, so that, by imposing the classical row-simplifying conditions (3.2), we are left with 10 degrees of freedom (Table 5).

0	0	0	0	0	0	0	0
c_2	c_2	0	0	0	0	0	0
c_3	$c_3 - \hat{a}_{32}$	\hat{a}_{32}	0	0	0	0	0
c_4	$c_4 - \hat{a}_{42} - \hat{a}_{43}$	\hat{a}_{42}	\hat{a}_{43}	0	0	0	0
c_5	$c_5 - \hat{a}_{52} - \hat{a}_{53} - \hat{a}_{54}$	\hat{a}_{52}	\hat{a}_{53}	\hat{a}_{54}	0	0	0
1	$1 - \hat{a}_{62} - \hat{a}_{63} - \hat{a}_{64} - \hat{a}_{65}$	\hat{a}_{62}	\hat{a}_{63}	\hat{a}_{64}	\hat{a}_{65}	0	0
	$1 - a_{62} - a_{63} - a_{64} - a_{65} - \gamma$	a_{62}	a_{63}	a_{64}	a_{65}	γ	0

Table 5: Butcher tableau of the explicit six-stage method.

The (remaining) order conditions (4.12), the coupling conditions (4.13), and the (remaining) supplementary order conditions (4.14) yield 10 conditions. However, one can verify that impos-

ing the order conditions and the supplementary order conditions (4.14a)-(4.14b), and taking into account the implicit companion method, the condition (4.14c) is automatically satisfied. Hence, following [51], and similarly to what we have done in Section 4.1, the remaining parameter is fixed by enlarging the stability region of the explicit method and imposing

$$\sum_{l,m,k,j} b_l \hat{a}_{lm} \hat{a}_{mk} \hat{a}_{kj} c_j = \frac{1}{135}.$$

Following the notation introduced in Section 4, the fourth-order schemes derived in this work are denoted by IMEX(4,6)-LDp, where LDp refers to the low-dispersion property of the implicit method. Specifically, we consider IMEX(4,6)-LDp₁ (Table 18), which, for the implicit companion method, is characterized by stage order 3 at the third intermediate stage and internal stability at the fourth and fifth (penultimate) stages. Next, we have IMEX(4,6)-LDp₂ (Table 19), which achieves stage order 3 at the third and fourth intermediate stages and internal stability at the fifth stage. Finally, IMEX(4,6)-LDp₃ (Table 20) is characterized by stage order 3 at the third, fourth, and fifth intermediate stages.

The difficulty of pursuing a general analytical treatment, together with the need to rely on numerical solvers to determine all coefficients, suggests that for higher-order schemes ($\ell > 4$) alternative approaches to time integration may be preferable. In particular, one may consider space-time variational discretizations [8], ADER methods, or deferred correction techniques [34, 46, 58, 60, 67]. However, these approaches are beyond the scope of the present work.

5 Polytopal discontinuous Galerkin method for space discretization

In this section, we introduce the space discretization using the polydG method [7, 27, 26]. First, let us introduce a polytopical mesh partition \mathcal{T}_h of the domain Ω made of disjoint polytopal elements K . For each element $K \in \mathcal{T}_h$, we denote by $|K|$ its d -dimensional measure. Concerning the space mesh regularity, we refer to the assumptions in [26, 27]. We define interface as the intersection of the $(d-1)$ -dimensional facets of two neighbouring elements. Namely, the facets are line segments and (planar) triangles decomposition of the polygons, for $d = 2$ and $d = 3$, respectively. We denote the set of facets as $\mathcal{F}_h = \mathcal{F}_h^I \cup \mathcal{F}_h^{Bh}$, where \mathcal{F}_h^I is the set of internal facets and \mathcal{F}_h^{Bh} the set of exterior ones. Finally, we split $\mathcal{F}_h^{Bh} = \mathcal{F}_h^D \cup \mathcal{F}_h^N$, where \mathcal{F}_h^D and \mathcal{F}_h^N are the boundary faces contained in Γ_D and Γ_N , respectively. We recall that we assume that $\Gamma_D \cap \Gamma_N = \emptyset$. Using the standard notation of Lebesgue and Sobolev spaces for scalar and vector-valued functions, we introduce the discontinuous finite element spaces

$$V_h^{\text{DG}} = \{v \in L^2(\Omega) : v|_K \in \mathbb{P}_\ell(K) \forall K \in \mathcal{T}_h, \quad \text{and} \quad \mathbf{V}_h^{\text{DG}} = [V_h^{\text{DG}}]^d,$$

where $\mathbb{P}_\ell(K)$ is the space of polynomials of total degree less than or equal to ℓ . Then, we introduce the trace operators [10] for a facet $F \in \mathcal{F}_h^I$ shared by the elements K^\pm . Let \mathbf{n}_{K^\pm} by the unit normal vector on face F pointing exterior to K^\pm , respectively. Then, for sufficiently regular scalar-valued functions w we define the average operator $\{\!\{ \cdot \}\!\}$ such that $\{\!\{ w \}\!\} = \frac{1}{2}(w|_{K^+} + w|_{K^-})$ and the jump operator $[\![\cdot]\!]$ such that $[\![w]\!] = w|_{K^+} \mathbf{n}_{K^+} + w|_{K^-} \mathbf{n}_{K^-}$. Analogously for a vector-valued function \mathbf{v} the definitions are $\{\!\{ \mathbf{v} \}\!\} = \frac{1}{2}(\mathbf{v}|_{K^+} + \mathbf{v}|_{K^-})$ and $[\![\mathbf{v}]\!] = \mathbf{v}|_{K^+} \cdot \mathbf{n}_{K^+} + \mathbf{v}|_{K^-} \cdot \mathbf{n}_{K^-}$. In the same way, on the face $F \in \mathcal{F}_h^D$ the average operators are defined as $\{\!\{ w \}\!\} = w|_K$ and $\{\!\{ \mathbf{v} \}\!\} = \mathbf{v}|_K$, while the

jump operators as $[[w]] = (w - g_D)|_K \mathbf{n}_K$ and $[[\mathbf{v}]] = (\mathbf{v} - \mathbf{g}_D)|_K \cdot \mathbf{n}_K$, where g_D and \mathbf{g}_D are the corresponding Dirichlet boundary conditions. We introduce the following dG-norm

$$\|\mathbf{u}\|_{\text{dG}}^2 = \sum_{j=1}^N \left(\|\sigma_j \nabla_h u_j\|_{\mathbf{L}^2(\Omega)}^2 + \sum_{F \in \mathcal{F}_h^I \cup \mathcal{F}_h^D} \|\sqrt{\eta_j} [[u_j]]\|_{\mathbf{L}^2(F)}^2 \right), \quad \forall \mathbf{u} \in \mathbf{V}_h^{\text{DG}},$$

where ∇_h is the elementwise gradient and $\eta_j : \mathcal{F}_h^I \cup \mathcal{F}_h^D \rightarrow \mathbb{R}_+$ is the penalization function defined as:

$$\eta_j = \eta_0 \begin{cases} \frac{\sigma_j \ell^2 |F|}{\{|K^\pm|\}_H}, & \text{on } F \in \mathcal{F}_h^I, \\ \frac{\sigma_j \ell^2 |F|}{|K|}, & \text{on } F \in \mathcal{F}_h^D. \end{cases} \quad (5.1)$$

In Equation (5.1), we are considering the harmonic average operator $\{a^\pm\}_H = \frac{2a^+a^-}{a^++a^-}$ on $F \in \mathcal{F}_h^I$, where a^+ and a^- are short notations for $a|_{K^+}$ and $a|_{K^-}$, respectively. Moreover, η_0 is a parameter to be chosen large enough to have stability [9]. Finally, we can define the following bilinear form

$\mathcal{A} : \mathbf{V}_h^{\text{DG}} \times \mathbf{V}_h^{\text{DG}} \rightarrow \mathbb{R}$ as $\mathcal{A}(\mathbf{u}, \mathbf{v}) = \sum_{j=1}^N \mathcal{A}_j(u_j, v_j)$, where

$$\begin{aligned} \mathcal{A}_j(u_j, v_j) &= \int_{\Omega} \sigma_j \nabla_h u_j \cdot \nabla_h v_j \, d\mathbf{x} + \sum_{F \in \mathcal{F}_h^I \cup \mathcal{F}_h^D} \int_F \eta_j [[u_j]] \cdot [[v_j]] \, d\boldsymbol{\sigma} \\ &\quad - \sum_{F \in \mathcal{F}_h^I \cup \mathcal{F}_h^D} \int_F (\{\{\sigma_j \nabla_h u_j\}\} \cdot [[v_j]] + \{\{\sigma_j \nabla_h v_j\}\} \cdot [[u_j]]) \, d\boldsymbol{\sigma}, \quad \forall \mathbf{u}, \mathbf{v} \in \mathbf{V}_h^{\text{DG}}. \end{aligned}$$

The semi-discrete PolyDG symmetric interior penalty formulation reads: for each $t \in (0, T]$ find $\mathbf{u}_h(t) \in \mathbf{V}_h^{\text{DG}}$ such that

$$\int_{\Omega} \dot{\mathbf{u}}_h(t) \mathbf{v}_h \, d\mathbf{x} + \mathcal{A}(\mathbf{u}_h(t), \mathbf{v}_h) = \int_{\Omega} \mathbf{F}(\mathbf{u}_h(t), t) \cdot \mathbf{v}_h \, d\mathbf{x} + \int_{\Gamma_N} \mathbf{g}_N \cdot \mathbf{v}_h \, d\boldsymbol{\sigma}, \quad \forall \mathbf{v}_h \in \mathbf{V}_h^{\text{DG}}, \quad (5.2a)$$

$$\mathbf{u}_h(0) = \mathbf{u}_{h0}, \quad \text{in } \Omega, \quad (5.2b)$$

where $\mathbf{u}_{h0} \in \mathbf{V}_h^{\text{DG}}$ is a suitable approximation of the initial condition \mathbf{u}_0 and we denote the time derivative with $\dot{\bullet} = \partial_t \bullet$. For more details about the derivation of the SIP-dG method for the laplacian term, we refer to [10]. Moreover, we refer to [5, 30], for the derivation of the method for two particular cases with $N = 1, 2$.

To derive the algebraic formulation of the system we introduce a suitable basis for each scalar equation $(\varphi_{jk})_{k=1}^M$ of the space V_h^{DG} such that $M = \dim(V_h^{\text{DG}})$. Then, we construct a vectorial basis $(\boldsymbol{\Phi}_k)_{k=1}^{NM}$ such that $\boldsymbol{\Phi}_k = [\varphi_k, 0, \dots, 0]^\top$ for $k = 1, \dots, M$, $\boldsymbol{\Phi}_{2k} = [0, \varphi_k, 0, \dots, 0]^\top$ for $k = M + 1, \dots, 2M$, and so on. Then we rewrite the solution

$$\mathbf{u}_h(\mathbf{x}, t) = \sum_{k=0}^{NM} U_k(t) \boldsymbol{\Phi}_k(\mathbf{x}),$$

where $\mathbf{U} \in \mathbb{R}^{NM}$ is the corresponding vector of the expansion coefficients written in terms of the

chosen basis. Moreover, we define the matrices and the vectors for $i, j = 1, \dots, NM$

$$[\mathbf{M}]_{ij} = \int_{\Omega} \Phi_j \cdot \Phi_i \, d\mathbf{x}, \quad (\text{Mass matrix}),$$

$$[\mathbf{K}]_{ij} = \mathcal{A}(\Phi_j, \Phi_i), \quad (\text{Stiffness matrix}),$$

$$[\mathbf{G}(\mathbf{U}(t))]_j = \int_{\Omega} \mathbf{F}(\mathbf{u}_h(t), t) \cdot \Phi_j \, d\mathbf{x}, \quad (\text{Nonlinear reaction vector}),$$

$$[\mathbf{G}_{\text{E,I}}(\mathbf{U}(t))]_j = \int_{\Omega} \mathbf{F}_{\text{E,I}}(\mathbf{u}_h(t), t) \cdot \Phi_j \, d\mathbf{x}, \quad (\text{Nonlinear reaction vectors for SI-IMEX}).$$

6 Numerical results: application to ODEs

The numerical methods and the IMEX-RK schemes presented in the previous sections are now validated through a series of test cases. While the ultimate goal of this work is the simulation of diffusion-reaction systems (2.1), the development of novel IMEX-RK schemes warrants a preliminary investigation on benchmark ODE problems. The tests of this section allow us to isolate and assess the fundamental properties of the proposed methods, including their accuracy and stability behaviour, and to compare them with existing approaches. More challenging diffusion-reaction applications are reported in Section 7. First, we consider a logistic ODE (or Verhulst model), which can be interpreted as a Fisher–Kolmogorov equation with vanishing diffusion. In the test case 2, we investigate the classical van der Pol oscillator [19, 45], a well-known stiff ODE problem.

For the reader’s convenience, Tables 6 and 7 summarize the third- and fourth-order IMEX-RK schemes employed in the numerical experiments, including both schemes available in the literature and those developed in the present work. The corresponding coefficients are reported in Appendix A. For each scheme, we indicate the number of stages and its main structural properties.

Scheme	Reference	Stages	Main features
IMEX-SSP(4, 3, 3)	[15]	4	Type I, L-stable, Strong stability preserving
IMEX-RK(4, 3, 3)	[18]	4	Type I, SA
BHR(5, 5, 3)	[14]	5	Type II, SA, condition (3.4), improved algebraic accuracy
ARK3(2)4L[2]SA	[49]	3	Type II, L-stable
IMEX(3, 5)-LDs ₁	present work	5	Type II, L-stable, condition (3.4), improved algebraic accuracy, triplet $[c_3^{(1-)}, c_4^{(1-)}, \hat{a}_{54}^{(1)}]$
IMEX(3, 5)-LDs ₂	present work	5	Type II, L-stable, condition (3.4), improved algebraic accuracy, triplet $[c_3^{(2)}, c_4^{(1-)}, \hat{a}_{54}^{(1)}]$
IMEX(3, 5)-LDp	present work	5	Type II, L-stable, condition (3.4), improved algebraic accuracy, triplet $[c_3^{(1-)}, c_4^{(1-)}, \hat{a}_{54}^{(2)}]$

Table 6: Third-order IMEX-RK schemes employed in the numerical simulations.

6.1 Test case 1: Verhulst model

As a first test case, we consider the Verhulst model. This is a single ODE, with a nonlinear quadratic term of the form

$$\frac{du}{dt} = \alpha u(1 - u),$$

supplemented with a suitable initial condition $u(0) = u_0$. As we will see in Section 7.1, this equation represents the limiting model of the Fisher–Kolmogorov equation in the absence of diffusion. The

Scheme	Reference	Stages	Main features
ARS(5, 5, 4)	[25]	5	Type ARS, SA
ARK4(3)6L[2]SA	[49]	6	Type II, L-stable
ARK4(3)7L[2]SA ₁	[51]	6	Type II, L-stable, condition (3.4)
IMEX(4, 6)-LDp ₁	present work	6	Type II, L-stable, condition (3.4), improved algebraic accuracy, low dispersion implicit method, stage order 3 3rd stage, internal stability 4th-5th stage
IMEX(4, 6)-LDp ₂	present work	6	Type II, L-stable, condition (3.4), improved algebraic accuracy, low dispersion implicit method, stage order 3 3rd-4th stage, internal stability 5th stage
IMEX(4, 6)-LDp ₃	present work	6	Type II, L-stable, condition (3.4), improved algebraic accuracy, low dispersion implicit method, stage order 3 3rd-4th-5th stage

Table 7: Fourth-order IMEX-RK schemes employed in the numerical simulations.

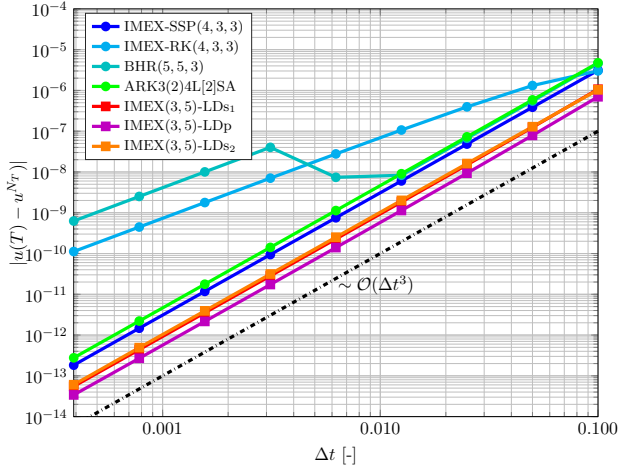
analytical solution is

$$u(t) = \frac{u_0 e^{\alpha t}}{1 + u_0 (e^{\alpha t} - 1)},$$

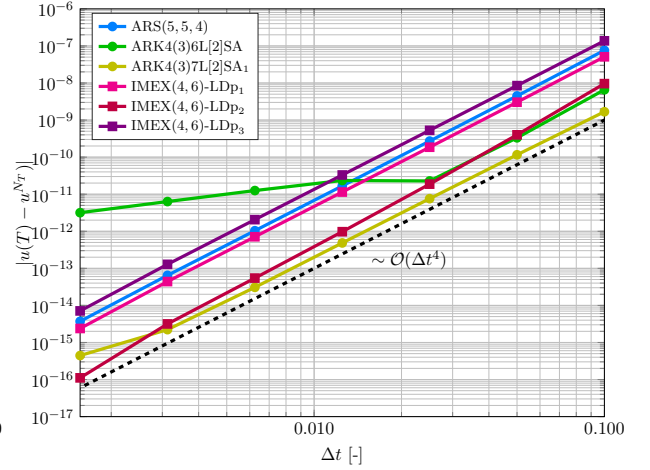
In the numerical experiments, we set $\alpha = 1$, $T = 1$, and $u_0 = 0.2$. According to the notation set in Section 3.1, the explicit and implicit components are given by $f_E = -\alpha u^2$ and $f_I = \alpha u$, respectively.

In Figure 1a, we show that the proposed third-order IMEX-RK schemes yield the smallest errors among all the tested methods. In particular, the combination $c_3^{(1-)}$ in (4.5) and $c_4^{(1-)}$ (4.6), which ensures stage order 3 at the third and fourth internal stages of the implicit companion method, yields lower errors. Overall, we identify three schemes that provide superior accuracy: IMEX(3, 5)-LDs₁ (Table 12), characterized by the triplet $[c_3^{(1-)}, c_4^{(1-)}, \hat{a}_{54}^{(1)}]$, IMEX(3, 5)-LDs₂ (Table 14), characterized by the triplet $[c_3^{(2)}, c_4^{(1-)}, \hat{a}_{54}^{(1)}]$, and IMEX(3, 5)-LDp (Table 13), characterized by the triplet $[c_3^{(1-)}, c_4^{(1-)}, \hat{a}_{54}^{(2)}]$. We recall that $c_3^{(2)}$ (4.9) guarantees stage order 2 for both the third and fourth explicit stage, while $\hat{a}_{54}^{(1)}$ (4.10) maximizes the order of dissipation of the explicit scheme, and $\hat{a}_{54}^{(2)}$ (4.11) maximizes the order of dispersion of the explicit scheme. Among these, IMEX(3, 5)-LDp produces the lowest error values.

Regarding the fourth-order schemes, Figure 1b shows that the proposed methods also perform very well. In particular, IMEX(4, 6)-LDp₂ (Table 19) attains the smallest errors, which are of the same order as those of the method by Kennedy and Carpenter [51], while requiring one stage fewer. This scheme is associated with stage order 3 for the third and fourth intermediate stage, while internal stability is enforced for the fifth (penultimate) internal stage, i.e. $R^{[5]}(\infty) = 0$, where $R^{[l]}$ denotes the stability function of the l -th stage.

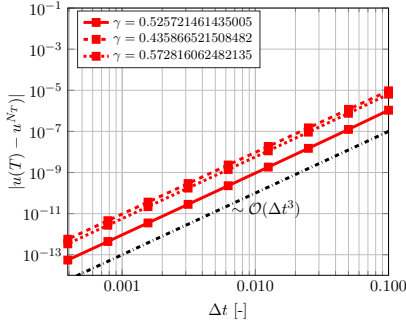


(a) Third-order methods

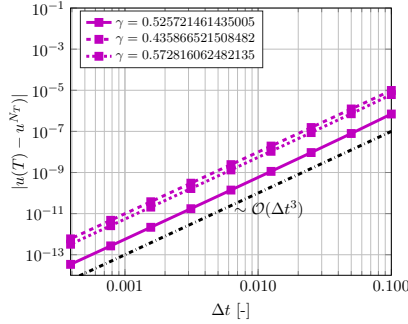


(b) Fourth-order methods

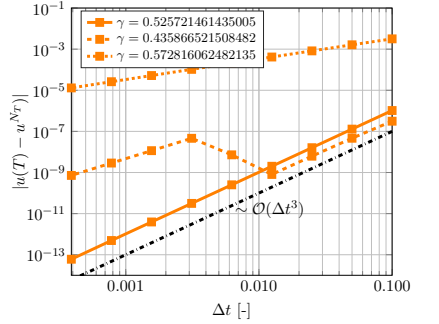
Figure 1: Test case 1, Verhulst model: convergence of different IMEX-RK schemes. The error is computed at final time for third-order (a) and fourth-order methods (b).



(a) IMEX(3, 5)-LDs₁



(b) IMEX(3, 5)-LDp



(c) IMEX(3, 5)-LDs₂

Figure 2: Test case 1, Verhulst model: comparison of three different versions of our method with $\gamma \simeq 0.5257$, derived in this work, $\gamma \simeq 0.4358$, classical literature choice, and $\gamma \simeq 0.5728$, obtained by maximizing the order of dissipation of the implicit method.

Additionally, we compare three versions of our method using three values of γ : $\gamma \simeq 0.5257$, derived here, the classical $\gamma \simeq 0.4358$ [14, 49], and $\gamma \simeq 0.5728$, obtained by maximizing the order of dissipation (see Section 4.1). Figure 2 shows that $\gamma \simeq 0.5257$ reduces errors by one order of magnitude for IMEX(3, 5)-LDs₁ and IMEX(3, 5)-LDp. For the IMEX(3, 5)-LDs₂ scheme, however, $\gamma \simeq 0.4358$ yields smaller errors at larger Δt , though they rise after 10^{-10} ; this issue does not occur with $\gamma \simeq 0.5257$. These findings indicate that the choice of γ may strongly affect the accuracy of the method, and that the selected value of γ improves the performance of the proposed third-order methods.

6.2 Van der Pol oscillator

The van der Pol's equation [14, 45] is one of the most widely studied nonlinear equations in the stiff ODE literature. It can be recast as the following first-order ODE system

$$\begin{aligned}\frac{du_1}{dt} &= u_2 \\ \frac{du_2}{dt} &= \frac{1}{\varepsilon} \left((1 - u_1^2) u_2 - u_1 \right),\end{aligned}$$

with $0 < \varepsilon \ll 1$. The IMEX-RK methods considered here treat the first equation explicitly and the second implicitly. This test problem is chosen to compare the accuracy of several types of IMEX-RK schemes and the new schemes in the presence of severe stiffness. In particular, the numerical experiments are performed with $\varepsilon = 10^{-6}$. Finally, following [14], we consider $T = 0.55139$ s and prescribe the initial conditions $u_1(0) = 2, u_2(0) = -\frac{2}{3} + \frac{10}{81}\varepsilon - \frac{292}{2187}\varepsilon^2 - \frac{1814}{19683}\varepsilon^3 + \mathcal{O}(\varepsilon^4)$.

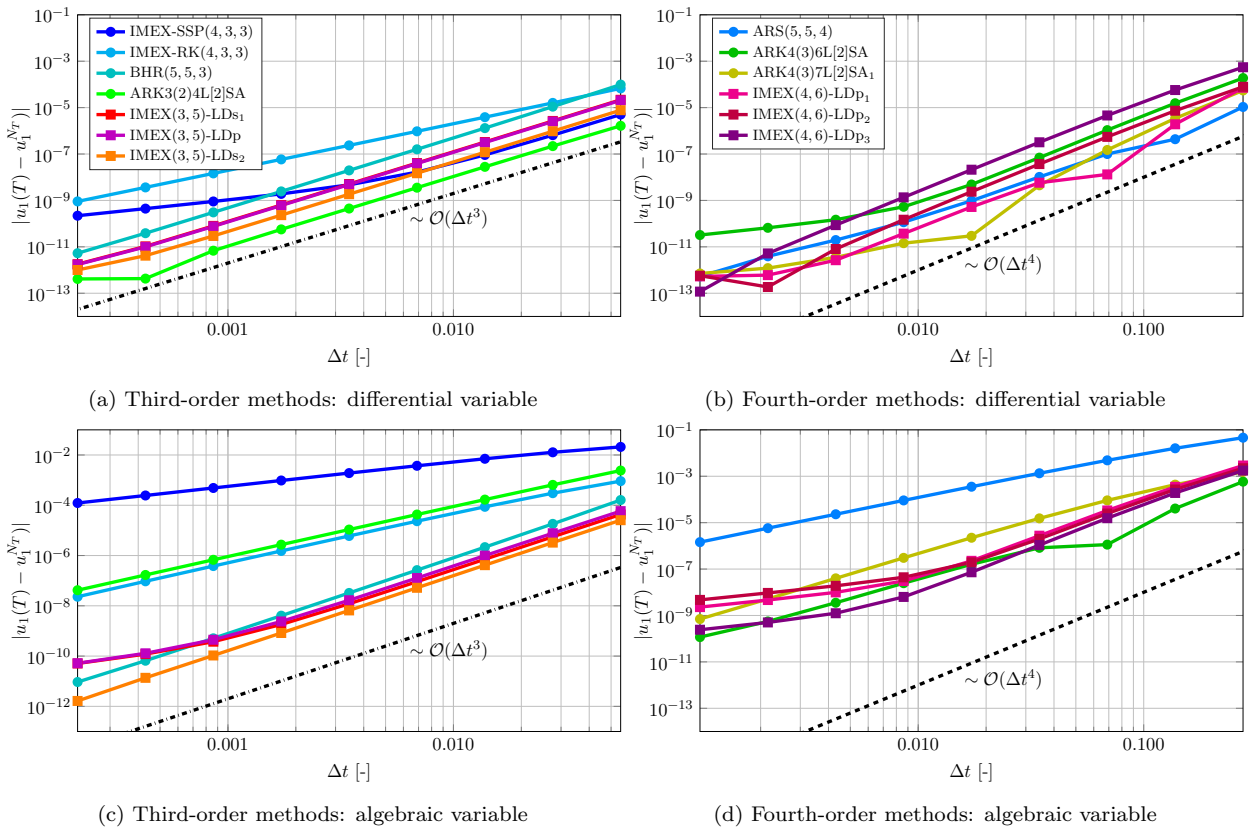


Figure 3: Test case 2, van der Pol oscillator: convergence of different IMEX-RK schemes. The error is computed at final time on the differential variable for third-order methods (a) and fourth-order methods (b), and on the algebraic variable for third-order methods (c) and fourth-order methods (d).

First, we compare the third-order IMEX-RK schemes on both the differential variable u_1 and the algebraic variable u_2 (see Figures 3a–3c). Some of the existing schemes from the literature exhibit noticeably larger global errors over the tested time-step range and show a more pronounced pre-asymptotic regime. In contrast, the Kennedy–Carpenter method from [49] and our new schemes display clean third-order convergence on both components. Moreover, on the algebraic variable our

schemes systematically deliver smaller errors than the Kennedy–Carpenter method at comparable time steps, so that they not only retain their nominal order but also provide a more accurate resolution of the stiff dynamics of the van der Pol system.

A similar behaviour is observed in the fourth-order comparison. The widely used ARS(5,5,4) method from [25] shows a loss of order and relatively large errors on the algebraic variable (see Figure 3d), whereas the ARK4(3)6LSA method from [49] suffers from a longer pre-asymptotic phase on the differential variable (see Figure 3b). In contrast, the three newly constructed fourth-order IMEX-RK schemes yield more robust error curves: they follow the expected fourth-order trend and only exhibit a loss of order in the algebraic component once the error in the differential variable falls below 10^{-12} , which is likely due to residual inaccuracies of the nonlinear solver that are difficult to reduce further in this stiff regime. Overall, the performance of the proposed methods is comparable to that of the ARK4(3)7L[2]SA₁ scheme in [51], while requiring one stage fewer.

7 Numerical results: application to PDEs

In this section, we present two applications of the IMEX methods to diffusion-reaction PDEs. First, we address the Fisher–Kolmogorov equation, a fundamental model in biological applications [28, 69], which admits travelling wave solutions [6, 28, 29]. Finally, we consider a two-species diffusion-reaction system, the so-called Gray–Scott model [44, 63], which exhibits complex patterns. The implementation of the polydG method described in Section 5 is carried out within the `lymph` library framework [4].

7.1 Travelling-wave solution of FK equation

In this section, we analyse the accuracy in simulating a travelling-wave solution of the Fisher–Kolmogorov (FK) problem. FK is a scalar problem ($n = 1$) that can be rewritten as in Equation (2.1), provided $F_1(u_1) = \alpha u_1(1 - u_1)$. Namely, considering $u = u_1$ and $\sigma = \sigma_1$, the FK model reads

$$\frac{\partial u}{\partial t} = \nabla \cdot (\sigma \nabla u) + \alpha u(1 - u) \quad \text{in } \Omega \times (0, T), \quad (7.1a)$$

$$\sigma \nabla u \cdot \mathbf{n}_\Omega = 0 \quad \text{on } \partial\Omega \times (0, T), \quad (7.1b)$$

$$u(\cdot, 0) = u_0 \quad \text{in } \Omega. \quad (7.1c)$$

Model (7.1) represents a simplified formulation of the so-called heterodimer model [69], which governs the dynamics of two different protein concentrations and is the classical mathematical description for neurodegenerative diseases. We refer, e.g., to [6, 28] for a more detailed discussion. In this section, we fix constant diffusion and reaction coefficients σ and α , and we consider travelling-wave solution of the form

$$u(x, y, t) = \psi(x - vt),$$

where v is wave speed depending on σ and α defined by $v := 5\sqrt{\alpha\sigma}/6$. Substituting u in the FK equation, we obtain an equivalent system of ODEs whose analytical solution is given by [70, §7.2]

$$\psi(x - vt) = \frac{1}{4} \left(1 + \tanh \left(8 - \sqrt{\frac{\alpha}{24\sigma}}(x - vt) \right) \right)^2.$$

This solution satisfies a homogeneous Neumann boundary condition at the limits $\xi \rightarrow \pm\infty$, which is equivalent to $x \rightarrow \pm\infty$ for each fixed value of $t \in (0, T]$. The homogeneous Neumann boundary condition is also respected in the y -direction, as the exact solution c is independent of y .

In this simulation, we consider a rectangular space domain $\Omega = (0, 3) \times (0, 1)$, and the final time $T = 4$. Homogeneous Neumann boundary conditions are imposed not only at $y = 0$ and $y = 1$, but also at $x = 0$ and $x = 3$. Concerning the physical parameters, we fix $\sigma = 10^{-3}$ and $\alpha = 1$. The resulting velocity associated with these values is $v \simeq 6.45 \times 10^{-2}$.

The computational domain is discretized with a fixed polygonal mesh consisting of 800 elements generated by PolyMesher [66]. The polynomial degree is set to $\ell = 8$ to emphasize the temporal errors associated with the IMEX time-integration scheme. We investigate temporal convergence by considering time steps $\Delta t = 0.8, 0.4, 0.2, 0.1$.

We also consider, for the first time in this test case, the SI-IMEX-RK approach presented in Section 3.2. To this end, we rewrite (7.1) in the form of a partitioned system (3.14) as follows

$$\frac{\partial u_E}{\partial t} = \nabla \cdot (\sigma \nabla u_I) + \alpha u_I (1 - u_E) \quad \text{in } \Omega \times (0, T), \quad (7.2)$$

$$\frac{\partial u_I}{\partial t} = \nabla \cdot (\sigma \nabla u_I) + \alpha u_I (1 - u_E) \quad \text{in } \Omega \times (0, T), \quad (7.3)$$

coupled with appropriate initial and boundary conditions as in (7.1). Following the discretization in Algorithm 1, u_E denotes the component treated explicitly, whereas u_I represents the component treated implicitly.

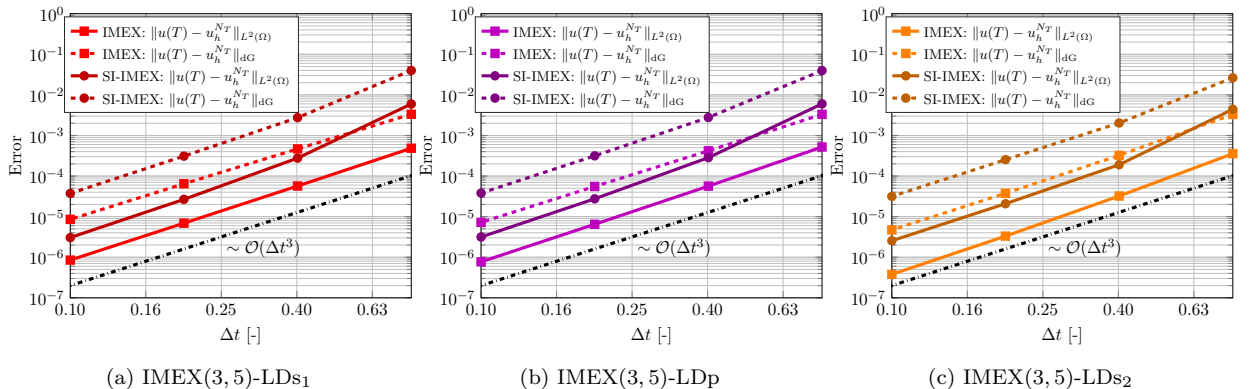


Figure 4: Test case 3, travelling-wave solution of FK equation: comparison of three different versions of our third-order method in the linearly implicit (IMEX) and semi-implicit (SI-IMEX) versions. The error is computed at final time both in $L^2(\Omega)$ and dG norms.

Figure 4 shows the error at the final time T as a function of the time-step size Δt for the three third-order IMEX-RK schemes proposed in this work. In each panel, we report the errors measured in the $L^2(\Omega)$ norm and in the dG norm, and we compare the standard linearly implicit IMEX formulation with its semi-implicit variant introduced in Section 3.2. The dashed reference line with slope three highlights the expected third-order convergence, which is clearly recovered by all schemes in the asymptotic regime.

The curves also show that the SI-IMEX methods tend to exhibit slightly larger error constants than their IMEX counterparts, while preserving the same temporal convergence rate. Moreover, we observe that the IMEX(3,5)-LDS2 scheme, which attains stage order 2 for both third and fourth order stage of the explicit part, yields the smallest errors in magnitude, in particular for the linearly implicit formulation.

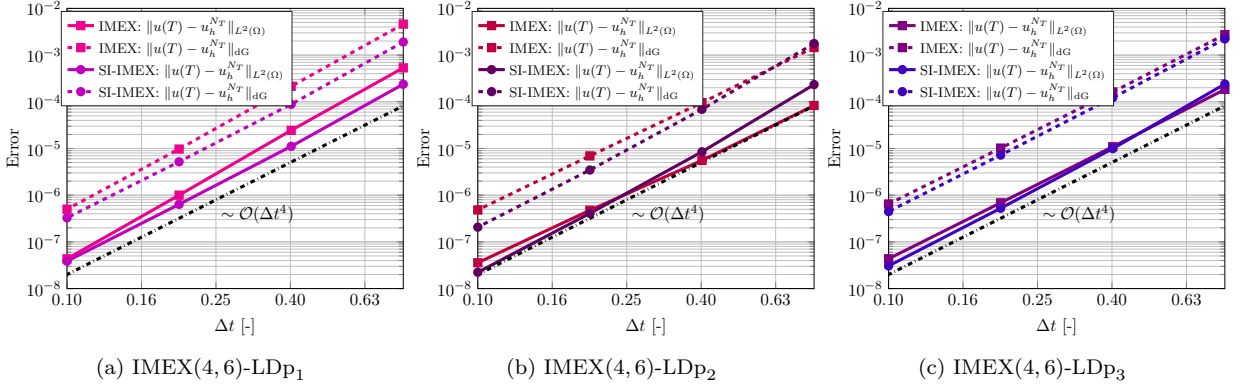


Figure 5: Test case 3, travelling-wave solution of FK equation: comparison of three different versions of our fourth-order method in the linearly implicit (IMEX) and semi-implicit (SI-IMEX) versions. The error is computed at final time both in $L^2(\Omega)$ and dG norms.

Figure 5 shows the error at the final time T as a function of the time-step size Δt for the three fourth-order IMEX-RK schemes presented in this work. The expected fourth-order convergence is clearly observed in the asymptotic regime for all schemes. The results indicate that all schemes yield errors of comparable magnitude. In addition, the plots show that, in this case, the SI-IMEX variants produce slightly smaller errors than their IMEX counterparts.

The observed behaviour may depend on the specific structure of the nonlinearity of the FK equation. The reaction term $\alpha u(1-u)$ is globally bounded and exhibits moderate nonlinear character, so that the discrepancy between the duplicated variables $u_E^{(n,l)}$ and $u_I^{(n,l)}$ at intermediate stages remains well-controlled. At fourth order, the increased accuracy of the stage approximations results in error constants that are comparable to, or even smaller than, those of the linearly implicit IMEX counterpart. At third order, however, the coarser stage representation seems to yield a more pronounced disagreement between $u_E^{(n,l)}$ and $u_I^{(n,l)}$, ultimately resulting in systematically larger error magnitudes despite the two formulations sharing the same asymptotic convergence rate.

7.2 Gray–Scott model

As a final test, we consider the Gray–Scott model [44, 63], which is widely used to study the formation of complex patterns arising from simple chemical reactions. The resulting reaction-diffusion system [63] can be cast in the form (2.1), by setting $\mathbf{u} = (u_1, u_2)^\top$, $\sigma_1 = \sigma_{u_1}$, $\sigma_2 = \sigma_{u_2}$, and

$$\mathbf{F}(\mathbf{u}, t) = (-u_1 u_2^2 + f(1 - u_1), u_1 u_2^2 - (f + k) u_2)^\top,$$

where f and k are characteristic (dimensionless) constant parameters of the the chemical reactions (see [63] for further details). Hence, we obtain

$$\frac{\partial u_1}{\partial t} = \nabla \cdot (\sigma_{u_1} \nabla u_1) - u_1 u_2^2 + f(1 - u_1) \quad \text{in } \Omega \times (0, T], \quad (7.4a)$$

$$\frac{\partial u_2}{\partial t} = \nabla \cdot (\sigma_{u_2} \nabla u_2) + u_1 u_2^2 - (f + k) u_2 \quad \text{in } \Omega \times (0, T], \quad (7.4b)$$

$$\sigma_{u_1} \nabla u_1 \cdot \mathbf{n}_\Omega = \sigma_{u_2} \nabla u_2 \cdot \mathbf{n}_\Omega = 0 \quad \text{on } \Omega \times (0, T], \quad (7.4c)$$

$$(u_1, u_2)(\cdot, 0) = (u_{1,0}, u_{2,0}) \quad \text{in } \Omega. \quad (7.4d)$$

The numerical simulation of the Gray–Scott model requires particular attention in the design of the time integration scheme. The diffusion forces fully explicit methods to adopt time steps $\Delta t = \mathcal{O}(h^2)$. Since the accurate resolution of localised patterns such as spots and travelling waves typically demands fine spatial meshes, this restriction renders long-time simulations computationally very expensive. High-order IMEX Runge–Kutta methods overcome this limitation by treating the diffusion operator implicitly and the nonlinear reaction term explicitly, allowing time steps substantially larger than the explicit stability bound, while preserving both the qualitative and quantitative structure of the Gray–Scott patterns. These patterns thus provide a particularly demanding benchmark for the schemes proposed in this work.

Due to the non-linearity, the term $u_1 u_2^2$ is treated explicitly, whereas the remaining terms are discretized implicitly. However, thanks to the linearity with respect to u_1 , the SI-IMEX-RK approach presented in Section 3.2 allows for an implicit discretization of u , i.e. of the linear factor in the nonlinear term $u_1 u_2^2$. In order to recast the system in the form (3.14), we introduce $(u_{1,E}, u_{2,E})^\top$ and $(u_{1,I}, u_{2,I})^\top$, and define

$$\mathbf{F}(\mathbf{u}_E, \mathbf{u}_I) = (-u_{1,I} u_{2,E}^2 + f(1 - u_{1,I}), u_{1,I} u_{2,E}^2 - (f + k)u_{2,I})^\top.$$

Hence, the resulting partitioned system writes

$$\frac{\partial u_{1,E}}{\partial t} = \nabla \cdot (\sigma_{u_1} \nabla u_{1,I}) - u_{1,I} u_{2,E}^2 + f(1 - u_{1,I}) \quad \text{in } \Omega \times (0, T], \quad (7.5a)$$

$$\frac{\partial u_{1,I}}{\partial t} = \nabla \cdot (\sigma_{u_1} \nabla u_{1,I}) - u_{1,I} u_{2,E}^2 + f(1 - u_{1,I}) \quad \text{in } \Omega \times (0, T], \quad (7.5b)$$

$$\frac{\partial u_{2,E}}{\partial t} = \nabla \cdot (\sigma_{u_2} \nabla u_{2,I}) + u_{1,I} u_{2,E}^2 - (f + k)u_{2,I} \quad \text{in } \Omega \times (0, T], \quad (7.5c)$$

$$\frac{\partial u_{2,I}}{\partial t} = \nabla \cdot (\sigma_{u_2} \nabla u_{2,I}) + u_{1,I} u_{2,E}^2 - (f + k)u_{2,I} \quad \text{in } \Omega \times (0, T], \quad (7.5d)$$

where Equation (7.5a) can be neglected in practical computations due to the absence of $u_{1,E}$ in the others.

For the numerical test we consider a two-dimensional square domain $\Omega = (0, 2.5)^2$ with diffusion coefficients $\sigma_{u_1} = 2 \times 10^{-5}$ and $\sigma_{u_2} = 10^{-5}$. For the spatial discretisation we consider a polynomial degree $\ell = 3$ on a cartesian mesh of 6 400 elements. The code is implemented in `lymph` [4]. As initial data we consider a steady state for the first variable $u_1 = 1$ and a localized square seeding for the second one $u_2 = 0.5$ in $\Omega_{\text{seed}} = \{(x, y) \in \mathbb{R}^2 : 1.1562 \leq x \leq 1.3438 \wedge 1.1562 \leq y \leq 1.3438\}$. To illustrate the ability of the scheme to reproduce qualitatively different dynamics until the maximum time $T = 5\,000$, we consider three choices of the reaction parameters [63]:

- $(f, k) = (0.030, 0.062)$, which produces a pattern of localised spots;
- $(f, k) = (0.037, 0.060)$, which generates labyrinthine structures;
- $(f, k) = (0.018, 0.051)$, which gives rise to the small-amplitude wave patterns.

In Figure 6, we report the results obtained using a time integration by means of the third-order IMEX(3, 5)-LDs₂ scheme with a time step $\Delta t = 1$. As visible from the results, the method provides an accurate resolution of the rich pattern-formation dynamics observed in the Gray–Scott system. In the first row (spots), a single initial bump destabilises into a ring of spots and then undergoes successive replications. In the second row (labyrinths), the initial annulus progressively folds and

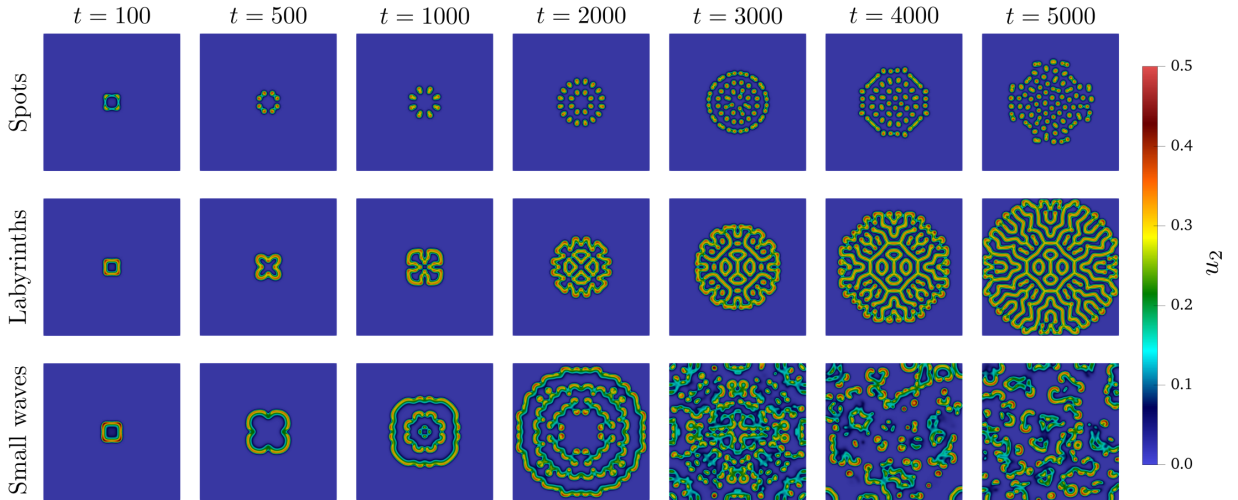


Figure 6: Test case 4, Gray–Scott model: numerical solutions at different times for three different values of the reaction parameters and with different patterns.

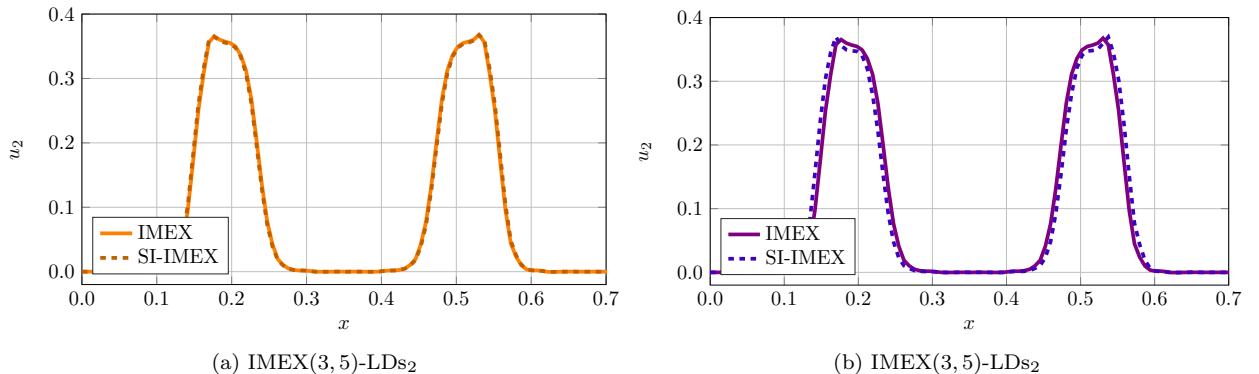


Figure 7: Test case 4, Gray–Scott model: profile of u_2 along the diagonal of the computational domain at $T = 200$ with $\Delta t = 0.5$. Comparison between the IMEX and SI-IMEX schemes for the third-order (a) and fourth-order (b).

branches into a connected labyrinthine network; the interfaces stay thin and smooth while the pattern coarsens, without spurious breakup or numerical artefacts. In the third row (small waves), the solution generates outward-propagating concentric waves that rapidly lose coherence and fragment into a disordered field of small-amplitude wavelets. The method is able to resolve the propagating fronts and their interactions without excessive smearing, so that individual crests remain clearly distinguishable throughout the simulation.

Moreover, to compare the accuracy and stability of the different strategies, we perform the same simulation up to $T = 200$ with parameters $(f, k) = (0.030, 0.062)$. In Figure 7, we report the profile of v_h along the diagonal connecting $(1, 1)$ to $(1.5, 1.5)$ in the computational domain, for both the third-order scheme IMEX(3,5)-LD s_2 and the fourth-order scheme IMEX(4,6)-LD p_3 for $\Delta t = 0.5$. We can see that for the third order, the IMEX and the SI-IMEX methods provide equivalent results. A small difference can be detected comparing the fourth-order methods.

In Figure 8, we report the profile of v_h for several values of the time step, namely $\Delta t \in \{0.5, 1.0, 2.0, 4.0, 8.0, 16.0\}$. For the standard IMEX formulations, the curves corresponding to

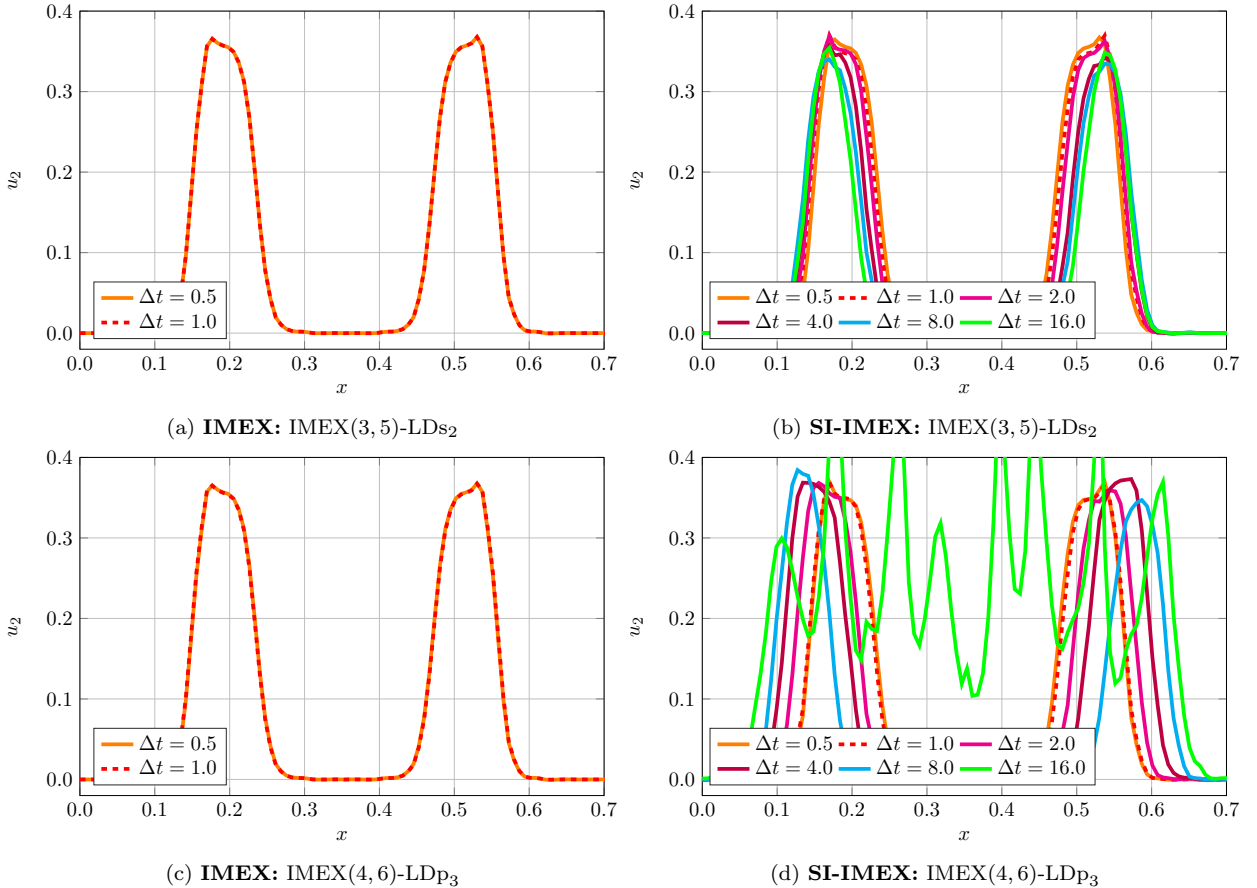


Figure 8: Test case 4, Gray–Scott model: profile of u_2 along the diagonal of the computational domain at $T = 200$ for several values of the time step Δt , computed with the third-order schemes IMEX (a) and SI-IMEX (b), and the fourth-order schemes IMEX (c) and SI-IMEX (d).

$\Delta t = 0.5$ and $\Delta t = 1.0$ are virtually indistinguishable, confirming that both the propagation speed and the shape of the travelling fronts are accurately captured at small time steps; however, the method becomes unstable for larger values of Δt and fails to produce a solution. In contrast, the SI-IMEX variants remain stable across the entire range of time steps considered, at the cost of a progressive deterioration of the wave profile: as Δt increases, phase shifts and shape distortions become visible, and are particularly pronounced for the fourth-order scheme.

8 Conclusions

In this work, we have presented IMplicit–EXplicit (IMEX) Runge–Kutta schemes coupled with a polytopal discontinuous Galerkin discretization for possibly degenerate diffusion–reaction problems. Since such models may admit travelling wave solutions, as in the Fisher–Kolmogorov equation, we have designed new third- and fourth-order IMEX–RK schemes tailored to improve the numerical description of wave propagation, with reduced artificial dissipation and dispersion. In addition, inspired by the partitioned formulation introduced in [15], we have proposed a new class of semi-implicit IMEX Runge–Kutta (SI-IMEX-RK) methods. This approach avoids a rigid separation between linear and nonlinear reaction components, while enabling the selective treatment of the

dominant (possibly linear) sources of stiffness. This strategy yields efficient and flexible schemes that can be naturally extended to more complex nonlinear dependencies, including those arising in the diffusion operator. The capabilities of the proposed methods have been assessed through a hierarchy of test cases of increasing complexity, targeting regimes characterized by strong stiffness and nonlinear dynamics. The experiments demonstrate that the considered schemes deliver accurate and stable solutions across a wide range of scenarios, including biologically relevant models.

Possible future directions of this work are the rigorous theoretical analysis of the SI-IMEX-RK framework, establishing entropy stability properties at the discrete level. A further promising direction is to couple the proposed time integration strategies with entropy-stable spatial discretisations based on summation-by-parts (SBP) operators [41, 42]. Extending these SBP constructions to general polygonal meshes and combining them with IMEX time stepping is a challenging but natural step towards fully structure-preserving numerical methods.

A Coefficients of employed IMEX-RK schemes

We report here, for the reader’s convenience, all the details on the IMEX–RK schemes employed in the numerical simulations, whose coefficients are approximated to the eighth decimal place. The interested reader may contact the authors to obtain the full-precision values.

A.1 Third-order schemes

Regarding the *third-order* schemes, we list here the schemes considered.

0	0	0	0	0
0.43586652	0.43586652	0	0	0
0.71793326	0.43586652	0.28206673	0	0
1	−0.73353408	2.15052738	−0.41699329	0
	0	1.20849664	−0.64436317	0.43586652
0.43586652	0.43586652	0	0	0
0.43586652	0	0.43586652	0	0
0.71793326	0	0.28206673	0.43586652	0
1	0	1.20849664	−0.64436317	0.43586652
	0	1.20849664	−0.64436317	0.43586652

Table 8: **Butcher tableaux of IMEX-RK(4,3,3) scheme employed in [18].** Explicit method (top) and implicit method (bottom).

0	0	0	0	0
0.87173304	0.87173304	0	0	0
0.60000000	0.52758901	0.07241098	0	0
1	0.39909600	-0.43755765	1.03846164	0
<hr/>				
	0.18764102	-0.59529747	0.97178992	0.43586652
0	0	0	0	0
0.87173304	0.43586652	0.43586652	0	0
0.60000000	0.25764824	-0.09351476	0.43586652	0
1	0.18764102	-0.59529747	0.97178992	0.43586652
<hr/>				
	0.18764102	-0.59529747	0.97178992	0.43586652

Table 9: **Butcher tableaux of ARK3(2)4L[2]SA scheme employed in [49].** Explicit method (top) and implicit method (bottom).

0	0	0	0	0	α	0	0	0	0
0	0	0	0	0	0	$-\alpha$	α	0	0
1	0	1	0	0	1	0	$1 - \alpha$	α	0
$\frac{1}{2}$	0	$\frac{1}{4}$	$\frac{1}{4}$	0	$\frac{1}{2}$	$\frac{\alpha}{4}$	η	$\frac{1}{2} - \frac{5}{4}\alpha - \eta$	α
<hr/>					<hr/>				
	0	$\frac{1}{6}$	$\frac{1}{6}$	$\frac{2}{3}$		0	$\frac{1}{6}$	$\frac{1}{6}$	$\frac{2}{3}$

Table 10: **Butcher tableaux of IMEX-SSP(4,3,3) scheme employed in [15].** Method with $\alpha = 0.24169426$ and $\eta = 0.12915286$. Explicit method (left) and implicit method (right).

0	0	0	0	0	0
0.87173304	0.87173304	0	0	0	0
0.87173304	0.43586652	0.43586652	0	0	0
0.65905793	-0.80099845	0	3.14121102	0	0
1	0.35675320	-0.19733989	0.88194884	-0.04136215	0
<hr/>					
	0.41289804	0	0.19733989	-0.04610445	0.43586652
0	0	0	0	0	0
0.87173304	0.43586652	0.43586652	0	0	0
0.87173304	0.43586652	0	0.43586652	0	0
0.65905793	-0.06675868	0	1.97110474	0.43586652	0
1	0.41289804	0	0.19733989	-0.04610445	0.43586652
<hr/>					
	0.41289804	0	0.19733989	-0.04610445	0.43586652

Table 11: **Butcher tableaux of BHR(5,5,3) scheme employed in [14].** Explicit method (top) and implicit method (bottom).

0	0	0	0	0	0
1.05144292	1.05144292	0	0	0	0
0.66658810	0.45528814	0.21129996	0	0	0
1.47683871	0.06936473	0	1.40747398	0	0
1	0.31801663	0.02902514	0.61071506	0.04224315	0
<hr/>					
	0.34225438	0.04450272	0.24901994	-0.16149852	0.52572146
0	0	0	0	0	0
1.05144292	0.52572146	0.52572146	0	0	0
0.66658810	0.26286073	-0.12199408	0.52572146	0	0
1.47683871	0.07706201	-0.69770293	1.57175818	0.52572146	0
1	0.34225438	0.04450272	0.24901994	-0.16149852	0.52572146
<hr/>					
	0.34225438	0.04450272	0.24901994	-0.16149852	0.52572146

Table 12: **Butcher tableaux of IMEX(3, 5)-LD_s₁ scheme.** Explicit method (top) and implicit method (bottom).

0	0	0	0	0	0
1.05144292	1.05144292	0	0	0	0
0.66658810	0.45528814	0.21129996	0	0	0
1.47683871	0.06936473	0	1.40747398	0	0
1	0.33449382	0.03977721	0.57503718	0.05069178	0
<hr/>					
	0.34225438	0.04450272	0.24901994	-0.16149852	0.52572146
0	0	0	0	0	0
1.05144292	0.52572146	0.52572146	0	0	0
0.66658810	0.26286073	-0.12199408	0.52572146	0	0
1.47683871	0.07706201	-0.69770293	1.57175818	0.52572146	0
1	0.34225438	0.04450272	0.24901994	-0.16149852	0.52572146
<hr/>					
	0.34225438	0.04450272	0.24901994	-0.16149852	0.52572146

Table 13: **Butcher tableaux of IMEX(3, 5)-LD_p scheme.** Explicit method (top) and implicit method (bottom).

0	0	0	0	0	0
1.05144292	1.05144292	0	0	0	0
0.60111815	0.42928617	0.17183197	0	0	0
1.26219537	-0.06294940	0	1.32514477	0	0
1	0.22291660	-0.00797809	0.72988821	0.05517327	0
<hr/>					
	0.28387977	0	0.40243695	-0.21203818	0.52572146
0	0	0	0	0	0
1.05144292	0.52572146	0.52572146	0	0	0
0.60111815	0.20412379	-0.12872709	0.52572146	0	0
1.26219537	0.12407344	-0.52211130	1.13451177	0.52572146	0
1	0.28387977	0	0.40243695	-0.21203818	0.52572146
<hr/>					
	0.28387977	0	0.40243695	-0.21203818	0.52572146

Table 14: **Butcher tableaux of IMEX(3,5)-LDs₂ scheme.** Explicit method (top) and implicit method (bottom).

A.2 Fourth-order schemes

Regarding the *fourth-order* schemes, we list here the schemes considered.

0	0	0	0	0	0	0	0	0	0	0	0	0	0
$\frac{1}{4}$	$\frac{1}{4}$	0	0	0	0	0	$\frac{1}{4}$	0	$\frac{1}{4}$	0	0	0	0
$\frac{3}{4}$	$-\frac{1}{4}$	1	0	0	0	0	$\frac{3}{4}$	0	$\frac{1}{2}$	$\frac{1}{4}$	0	0	0
$\frac{11}{20}$	$-\frac{13}{100}$	$\frac{43}{75}$	$\frac{8}{75}$	0	0	0	$\frac{11}{20}$	0	$\frac{17}{50}$	$-\frac{1}{25}$	$\frac{1}{4}$	0	0
$\frac{1}{2}$	$-\frac{6}{85}$	$\frac{42}{85}$	$\frac{179}{1360}$	$-\frac{15}{272}$	0	0	$\frac{1}{2}$	0	$\frac{371}{1360}$	$-\frac{137}{2720}$	$\frac{15}{544}$	$\frac{1}{4}$	0
1	0	$\frac{79}{24}$	$-\frac{5}{8}$	$\frac{25}{2}$	$-\frac{85}{6}$	0	1	0	$\frac{25}{24}$	$-\frac{49}{48}$	$\frac{125}{16}$	$-\frac{85}{12}$	$\frac{1}{4}$
<hr/>							<hr/>						
	0	$\frac{25}{24}$	$-\frac{49}{48}$	$\frac{125}{16}$	$-\frac{85}{12}$	$\frac{1}{4}$		0	$\frac{25}{24}$	$-\frac{49}{48}$	$\frac{125}{16}$	$-\frac{85}{12}$	$\frac{1}{4}$

Table 15: **Butcher tableaux of IMEX-ARS(5,5,4) scheme employed in [15].** Explicit method (left) and implicit method (right).

0	0	0	0	0	0	0
0.50000000	0.50000000	0	0	0	0	0
0.33200000	0.22177600	0.11022400	0	0	0	0
0.62000000	-0.04884659	-0.17772065	0.84656724	0	0	0
0.85000000	-0.15541685	-0.35670501	1.05872588	0.30339599	0	0
1	0.20142435	0.00874206	0.15993996	0.40382906	0.22606457	0
<hr/>						
	0.15791629	0	0.18675894	0.68056529	-0.27524053	0.25000000
0	0	0	0	0	0	0
0.50000000	0.25000000	0.25000000	0	0	0	0
0.33200000	0.13777600	-0.05577600	0.25000000	0	0	0
0.62000000	0.14463687	-0.22393190	0.44929504	0.25000000	0	0
0.85000000	0.09825878	-0.59154424	0.81012105	0.28316440	0.25000000	0
1	0.15791629	0	0.18675894	0.68056529	-0.27524053	0.25000000
<hr/>						
	0.15791629	0	0.18675894	0.68056529	-0.27524053	0.25000000

Table 16: **Butcher tableaux of ARK4(3)6L[2]SA scheme employed in [49].** Explicit method (top) and implicit method (bottom).

0	0	0	0	0	0	0	0
2γ	2γ	0	0	0	0	0	0
0.42165537	0.06175000	0.35990537	0	0	0	0	0
0.33500000	0.05301658	0.35949264	-0.07750923	0	0	0	0
0.07500000	0.05841715	-0.16313824	-0.19732090	0.37704199	0	0	0
0.70000000	0.53853032	-0.45497746	1.25629056	-0.47828452	-0.16155888	0	0
1	0.23221715	0.23221715	-6.80999437	7.36185855	-1.37487908	1.35858058	0
<hr/>							
	0	0	0.51611072	-0.14606356	0.23473048	0.27172234	γ
0	0	0	0	0	0	0	0
2γ	γ	γ	0	0	0	0	0
0.42165537	0.14907768	0.14907768	γ	0	0	0	0
0.33500000	0.12483442	0.12483442	-0.03816885	γ	0	0	0
0.07500000	-0.07303194	-0.07303194	-0.24343569	0.34099956	γ	0	0
0.70000000	-0.15296500	-0.15296500	0.07220562	0.40430630	0.40591807	γ	0
	0	0	0.51611072	-0.14606356	0.23473048	0.27172234	γ
<hr/>							
	0	0	0.51611072	-0.14606356	0.23473048	0.27172234	γ

Table 17: **Butcher tableaux of ARK4(3)7L[2]SA₁ scheme employed in [51].** Method with $\gamma = 0.1235$. Explicit method (top) and implicit method (bottom).

0	0	0	0	0	0	0
0.55610768	0.55610768	0	0	0	0	0
1.31576490	-0.33180581	1.64757071	0	0	0	0
0.08673938	0.13811029	-0.00270761	-0.04866330	0	0	0
0.43558989	1.03496518	0.54237034	-0.07939527	-1.06235036	0	0
1	-1.25469717	-0.59939455	0.17680815	1.62106030	1.05622327	0
	-1.25469717	-0.59939455	0.17680815	1.62106030	1.05622327	0
0	0	0	0	0	0	0
0.55610768	0.27805384	0.27805384	0	0	0	0
1.31576490	0.13902692	0.89868414	0.27805384	0	0	0
0.08673938	-0.12975100	-0.07983424	0.01827080	0.27805384	0	0
0.43558989	-0.14018717	-0.12525399	0.00546592	0.41751129	0.27805384	0
1	0.09317511	0	-0.03410445	0.06284142	0.60003407	0.27805384
	0.09317511	0	-0.03410445	0.06284142	0.60003407	0.27805384

Table 18: **Butcher tableaux of IMEX(4, 6)-LD p_1 scheme.** Explicit method (top) and implicit method (bottom).

0	0	0	0	0	0	0
0.55610768	0.55610768	0	0	0	0	0
0.35255814	0.04247560	0.31008254	0	0	0	0
0.66303019	0.40040468	-0.03002200	0.29268752	0	0	0
0.89332539	0.52440469	-0.72698360	0.23689320	0.85901111	0	0
1	0.23510769	-1.18401116	0.30313013	1.81785990	-0.17208657	0
	0.23510769	-1.18401116	0.30313013	1.81785990	-0.17208657	0
0	0	0	0	0	0	0
0.55610768	0.27805384	0.27805384	0	0	0	0
0.35255814	0.13902692	-0.06452261	0.27805384	0	0	0
0.66303019	0.09279114	-0.33193809	0.62412330	0.27805384	0	0
0.89332539	-0.06208062	-0.96963964	1.29531364	0.35167818	0.27805384	0
1	0.14889680	0	0.29346325	0.57004255	-0.29045645	0.27805384
	0.14889680	0	0.29346325	0.57004255	-0.29045645	0.27805384

Table 19: **Butcher tableaux of IMEX(4, 6)-LD p_2 scheme.** Explicit method (top) and implicit method (bottom).

0	0	0	0	0	0	0
0.55610768	0.55610768	0	0	0	0	0
0.35255814	0.31554253	0.03701561	0	0	0	0
0.66303019	0.04611287	-0.49427752	1.11119485	0	0	0
0.03422808	0.10180581	0.05442689	-0.14018574	0.01818112	0	0
1	-2.05008320	-1.19976062	0.13177740	1.55817443	2.55989198	0
<hr/>						
	-2.05008320	-1.19976062	0.13177740	1.55817443	2.55989198	0
0	0	0	0	0	0	0
0.55610768	0.27805384	0.27805384	0	0	0	0
0.35255814	0.13902692	-0.06452261	0.27805384	0	0	0
0.66303019	0.0927911	-0.33193809	0.62412330	0.27805384	0	0
0.03422808	-0.20769213	-0.01432779	-0.04346364	0.02165781	0.27805384	0
1	4.03283234	0	1.76674922	-0.36122323	-4.71641218	0.27805384
<hr/>						
1	4.03283234	0	1.76674922	-0.36122323	-4.71641218	0.27805384

Table 20: **Butcher tableaux of IMEX(4, 6)-LDp₃ scheme.** Explicit method (top) and implicit method (bottom).

B Derivation of index-1 DAE supplementary conditions up to order 4

We consider the singularly perturbed system

$$\begin{aligned} y'(t) &= f(y(t), z(t)), \\ \varepsilon z'(t) &= g(y(t), z(t)), \end{aligned} \tag{B.1}$$

with $0 < \varepsilon \ll 1$ and $g_z(y, z)$ invertible on the region of interest (*index-1* DAE case). We focus on schemes of type I and we assume \mathbf{A} invertible, so that $\mathbf{w} = \mathbf{A}^{-1}$. The derived relations will be valid for schemes of type II by considering $\omega = \mathcal{A}^{-1}$ [14], that is assumed to be invertible. An IMEX-RK scheme of type I applied to the reduced DAE reads [13]

$$y^{(n,l)} = y^n + \Delta t \sum_{m=1}^s \hat{a}_{lm} f(y^{(n,m)}, z^{(n,m)}), \tag{B.2a}$$

$$0 = g(y^{(n,m)}, z^{(n,m)}), \tag{B.2b}$$

$$y^{n+1} = y^n + \Delta t \sum_{l=1}^s \hat{b}_l f(y^{(n,l)}, z^{(n,l)}) \tag{B.2c}$$

$$z^{n+1} = \rho z^n + \Delta t \sum_{l,m=1}^s b_l w_{lm} z^{(n,m)}, \tag{B.2d}$$

where $\rho = R(\infty) < 1$. We need to compute the local truncation error Δz^{n+1} . We drop the explicit dependence on time, all the quantities are evaluated at time t^n (subscript n). First, we recall the Taylor expansion of the exact solution

$$z_{n+1} = z_n + \Delta t z'_n + \frac{\Delta t^2}{2} z''_n + \frac{\Delta t^3}{6} z'''_n + \mathcal{O}(\Delta t^4). \tag{B.3}$$

We introduce for the sake of convenience

$$\mathcal{Z}_{1,n} = -g_{z,n}^{-1} g_{y,n} \tag{B.4a}$$

$$\mathcal{Z}_{2,n} = -g_{z,n}^{-1} (g_{yy,n} + 2g_{yz,n}\mathcal{Z}_{1,n} + g_{zz,n}\mathcal{Z}_{1,n}^2) \tag{B.4b}$$

$$\mathcal{Z}_{3,n} = -g_{z,n}^{-1} (g_{yyy,n} + 3g_{yyz,n}\mathcal{Z}_{1,n} + 3g_{yzz,n}\mathcal{Z}_{1,n}^2 + g_{zzz,n}\mathcal{Z}_{1,n}^3 + 3g_{yz,n}\mathcal{Z}_{2,n} + 3g_{zz,n}\mathcal{Z}_{1,n}\mathcal{Z}_{2,n}), \tag{B.4c}$$

so that

$$\begin{aligned} z'_n &= \mathcal{Z}_{1,n} y'_n = \mathcal{Z}_{1,n} f_n, \\ z''_n &= \mathcal{Z}_{1,n} y''_n + \mathcal{Z}_{2,n} (y'_n)^2 = \mathcal{Z}_{1,n} y''_n + \mathcal{Z}_{2,n} f_n^2 \\ &= -g_{z,n}^{-1} \left(\underbrace{g_{y,n} (f_{y,n} f_n + f_{z,n} z'_n)}_{\text{first-order derivatives block}} \right. \\ &\quad \left. + \underbrace{g_{yy,n} f_n^2 + 2g_{yz,n} f_n z'_n + g_{zz,n} (z'_n)^2}_{\text{second-order derivatives block}} \right) \\ z'''_n &= \mathcal{Z}_{1,n} y'''_n + 3\mathcal{Z}_{2,n} y'_n y''_n + \mathcal{Z}_3 (y'_n)^3 = \mathcal{Z}_{1,n} y'''_n + 3\mathcal{Z}_{2,n} f_n y''_n + \mathcal{Z}_{3,n} f_n^3 \\ &= -g_{z,n}^{-1} \left(\underbrace{g_{y,n} (f_{y,n} (f_{y,n} f_n + f_{z,n} z'_n) + f_{z,n} z''_n + f_{yy,n} f_n^2 + 2f_{yz,n} f_n z'_n + f_{zz,n} z_n'^2)}_{\text{first-order derivatives block}} \right. \\ &\quad \left. + 3 \underbrace{(g_{yy,n} f_n (f_{y,n} f_n + f_{z,n} z'_n) + g_{yz,n} (z'_n (f_{y,n} f_n + f_{z,n} z'_n) + f_n z''_n) + g_{zz,n} z'_n z''_n)}_{\text{second-order derivatives block}} \right. \\ &\quad \left. + \underbrace{g_{yyy,n} f_n^3 + 3g_{yyz,n} f_n^2 z'_n + 3g_{yzz,n} f_n (z'_n)^2 + g_{zzz,n} (z'_n)^3}_{\text{third-order derivatives block}} \right) \\ &= -g_{z,n}^{-1} \left(\underbrace{g_{y,n} (f_{y,n} (f_{y,n} f_n + f_{z,n} z'_n) + f_{z,n} z''_n + f_{yy,n} f_n^2 + 2f_{yz,n} f_n z'_n + f_{zz,n} z_n'^2)}_{\text{first-order derivatives block}} \right. \\ &\quad \left. + 3 \underbrace{(g_{yy,n} f_n (f_{y,n} f_n + f_{z,n} z'_n) + g_{yz,n} (2z'_n (f_{y,n} f_n + f_{z,n} z'_n) + \mathcal{Z}_{2,n} f_n^3) + g_{zz,n} z'_n z''_n)}_{\text{second-order derivatives block}} \right. \\ &\quad \left. + \underbrace{g_{yyy,n} f_n^3 + 3g_{yyz,n} f_n^2 z'_n + 3g_{yzz,n} f_n (z'_n)^2 + g_{zzz,n} (z'_n)^3}_{\text{third-order derivatives block}} \right). \end{aligned}$$

Notice in particular that

$$\begin{aligned} g_{yz,n} (z'_n (f_{y,n} f_n + f_{z,n} z'_n) + f_n z''_n) &= g_{yz,n} (z'_n y''_n + f_n z''_n) \\ &= g_{yz,n} (\mathcal{Z}_{1,n} f_n y''_n + f_n (\mathcal{Z}_{1,n} y''_n + \mathcal{Z}_{2,n} f_n^3)) \\ &= g_{yz,n} (2\mathcal{Z}_{1,n} f_n y''_n + \mathcal{Z}_{2,n} f_n^3) \end{aligned}$$

and that

$$z'_n z''_n = z'_n (\mathcal{Z}_{1,n} y''_n + \mathcal{Z}_{2,n} f_n^2) = \mathcal{Z}_{1,n}^2 f_n y''_n + \mathcal{Z}_{1,n} \mathcal{Z}_{2,n} f_n^3.$$

In order to compute the Taylor expansion of the numerical method at time t^n we need to compute the Taylor expansion of the intermediate stages $z^{(n,m)}$. These are defined implicitly,

through the relation $g(y^{(n,m)}, z^{(n,m)}) = 0$, so that

$$\begin{aligned}
0 &= g(y^{(n,m)}, z^{(n,m)}) = g(y_n + \Delta y^{(n,m)}, z_n + \Delta z^{(n,m)}) \\
&= \underbrace{g_n}_{=g(y_n, z_n)=g(y^{(n)}, z^{(n)})=0} + g_{y,n} \Delta y^{(n,m)} + g_{z,n} \Delta z^{(n,m)} \\
&+ \frac{1}{2} g_{yy,n} \left(\Delta y^{(n,m)} \right)^2 + g_{yz,n} \Delta y^{(n,m)} \Delta z^{(n,m)} + \frac{1}{2} g_{zz,n} \left(\Delta z^{(n,m)} \right)^2 \\
&+ \frac{1}{6} g_{yyy,n} \left(\Delta y^{(n,m)} \right)^3 + \frac{1}{2} g_{yyz,n} \left(\Delta y^{(n,m)} \right)^2 \Delta z^{(n,m)} + \frac{1}{2} g_{yzz,n} \Delta y^{(n,m)} \left(\Delta z^{(n,m)} \right)^2 \\
&+ \frac{1}{6} g_{zzz,n} \left(\Delta z^{(n,m)} \right)^3 + \mathcal{O} \left(\Delta y^{(n,m)} \right)^4 + \mathcal{O} \left(\Delta z^{(n,m)} \right)^4,
\end{aligned} \tag{B.5}$$

so that, by defining

$$\Delta z^{(n,m)} = \Delta z^{(n,m),1} + \Delta z^{(n,m),2} + \Delta z^{(n,m),3} + \mathcal{O}(\Delta t^4)$$

one obtains

$$\Delta z^{(n,m),1} = -g_{z,n}^{-1} g_{y,n} \Delta y^{(n,m),1}, \tag{B.6a}$$

$$\Delta z^{(n,m),2} = -g_{z,n}^{-1} \left(g_{y,n} \Delta y^{(n,m),2} + \frac{1}{2} g_{yy,n} \left(\Delta y^{(n,m),1} \right)^2 + g_{yz,n} \Delta y^{(n,m),1} \Delta z^{(n,m),1} + \frac{1}{2} g_{zz,n} \left(\Delta z^{(n,m),1} \right)^2 \right), \tag{B.6b}$$

$$\begin{aligned}
\Delta z^{(n,m),3} &= -g_{z,n}^{-1} \left(g_{y,n} \Delta y^{(n,m),3} + g_{yy,n} \Delta y^{(n,m),1} \Delta y^{(n,m),2} + g_{zz,n} \Delta z^{(n,m),1} \Delta z^{(n,m),2} \right. \\
&+ g_{yz,n} \Delta y^{(n,m),1} \Delta z^{(n,m),2} + g_{yz,n} \Delta y^{(n,m),2} \Delta z^{(n,m),1} \\
&+ \frac{1}{6} g_{yyy,n} \left(\Delta y^{(n,m),1} \right)^3 + \frac{1}{6} g_{zzz,n} \left(\Delta z^{(n,m),1} \right)^3 \\
&\left. + \frac{1}{2} g_{yyz,n} \left(\Delta y^{(n,m),1} \right)^2 \Delta z^{(n,m),1} + \frac{1}{2} g_{yzz,n} \Delta y^{(n,m),1} \left(\Delta z^{(n,m),1} \right)^2 \right).
\end{aligned} \tag{B.6c}$$

Now we need to compute the expansions of $\Delta y^{(n,m)}$, so that

$$\Delta y^{(n,m)} = \Delta y^{(n,m),1} + \Delta y^{(n,m),2} + \Delta y^{(n,m),3} + \mathcal{O}(\Delta t^4).$$

In order to achieve this goal, we need to consider the expansion of f

$$\begin{aligned}
f(y^{(n,m)}, z^{(n,m)}) &= f_n + f_{y,n} \Delta y^{(n,m)} + f_{z,n} \Delta z^{(n,m)} \\
&+ \frac{1}{2} f_{yy,n} \left(\Delta y^{(n,m)} \right)^2 + f_{yz,n} \Delta y^{(n,m)} \Delta z^{(n,m)} + \frac{1}{2} f_{zz,n} \left(\Delta z^{(n,m)} \right)^2 \\
&+ \frac{1}{6} f_{yyy,n} \left(\Delta y^{(n,m)} \right)^3 + \frac{1}{2} f_{yyz,n} \left(\Delta y^{(n,m)} \right)^2 \Delta z^{(n,m)} \\
&+ \frac{1}{2} f_{yzz,n} \Delta y^{(n,m)} \left(\Delta z^{(n,m)} \right)^2 + \frac{1}{6} f_{zzz,n} \left(\Delta z^{(n,m)} \right)^3
\end{aligned} \tag{B.7}$$

More specifically, we obtain

Order 1 (Δt)

$$\Delta y^{(n,m),1} = \Delta t \sum_k \hat{a}_{mk} f_n = \Delta t \hat{c}_m f_n, \tag{B.8}$$

Order 2 (Δt^2)

$$\Delta y^{(n,m),2} = \Delta t \sum_k \hat{a}_{mk} \left(f_{y,n} \Delta y^{(n,k),1} + f_{z,n} \Delta z^{(n,k),1} \right), \quad (\text{B.9})$$

Order 3 (Δt^3)

$$\begin{aligned} \Delta y^{(n,m),3} = \Delta t \sum_k \hat{a}_{mk} & \left(f_{y,n} \Delta y^{(n,k),2} + f_{z,n} \Delta z^{(n,k),2} \right. \\ & \left. + \frac{1}{2} f_{yy,n} (\Delta y^{(n,k),1})^2 + f_{yz,n} \Delta y^{(n,k),1} \Delta z^{(n,k),1} + \frac{1}{2} f_{zz,n} (\Delta z^{(n,k),1})^2 \right). \end{aligned} \quad (\text{B.10})$$

By successive substitution, we obtain

Order 1 (Δt)

$$\Delta z^{(n,m),1} = \mathcal{Z}_{1,n} \Delta y^{(n,m),1} = -\Delta t g_{z,n}^{-1} g_{y,n} \hat{c}_m f_n = \Delta t \hat{c}_m z'_n. \quad (\text{B.11})$$

Order 2 (Δt^2)

$$\Delta y^{(n,m),2} = \Delta t \sum_k \hat{a}_{mk} \left(f_{y,n} \Delta y^{(n,k),1} + f_{z,n} \mathcal{Z}_{1,n} \Delta y^{(n,k),1} \right) = \Delta t^2 \sum_k \hat{a}_{mk} \hat{c}_k (f_{y,n} f_n + f_{z,n} z'_n) \quad (\text{B.12a})$$

$$\begin{aligned} \Delta z^{(n,m),2} &= \mathcal{Z}_{1,n} \Delta y^{(n,m),2} + \frac{1}{2} \mathcal{Z}_{2,n} (\Delta y^{(n,m),1})^2 \\ &= -g_{z,n}^{-1} \left[g_{y,n} \Delta y^{(n,m),2} + \frac{1}{2} (g_{yy,n} + 2g_{yz,n} \mathcal{Z}_{1,n} + g_{zz,n} \mathcal{Z}_{1,n}^2) (\Delta y^{(n,m),1})^2 \right] \\ &= -\Delta t^2 g_{z,n}^{-1} \left(\underbrace{\sum_k \hat{a}_{mk} \hat{c}_k g_{y,n} (f_{y,n} f_n + f_{z,n} z'_n)}_{\text{first-order derivatives block}} + \underbrace{\frac{\hat{c}_m^2}{2} (g_{yy,n} f_n^2 + 2g_{yz,n} f_n z'_n + g_{zz,n} (z'_n)^2)}_{\text{second-order derivatives block}} \right). \end{aligned} \quad (\text{B.12b})$$

Order 3 (Δt^3)

$$\begin{aligned} \Delta y^{(n,m),3} &= \Delta t \sum_k \hat{a}_{mk} \left(f_{y,n} \Delta y^{(n,k),2} + f_{z,n} \left(\mathcal{Z}_{1,n} \Delta y^{(n,k),2} + \frac{1}{2} \mathcal{Z}_{2,n} (\Delta y^{(n,k),1})^2 \right) \right. \\ & \quad \left. + \frac{1}{2} (\Delta y^{(n,k),1})^2 (f_{yy,n} + 2f_{yz,n} \mathcal{Z}_{1,n} + f_{zz,n} \mathcal{Z}_{1,n}^2) \right) \\ &= \Delta t \sum_k \hat{a}_{mk} \left(f_{y,n} \Delta y^{(n,k),2} + f_{z,n} \left(\mathcal{Z}_{1,n} \Delta y^{(n,k),2} + \frac{1}{2} \mathcal{Z}_{2,n} (\Delta y^{(n,k),1})^2 \right) \right. \\ & \quad \left. + \Delta t^2 \frac{\hat{c}_k^2}{2} (f_{yy,n} f_n^2 + 2f_{yz,n} f_n z'_n + f_{zz,n} z_n'^2) \right) \\ &= \Delta t^3 \sum_k \hat{a}_{mk} \left[\underbrace{\sum_j \hat{a}_{kj} \hat{c}_j (f_{y,n} + f_{z,n} \mathcal{Z}_{1,n}) (f_{y,n} f_n + f_{z,n} z'_n)}_{\text{first-order derivatives block}} + \frac{\hat{c}_k^2}{2} f_{z,n} \mathcal{Z}_{2,n} f_n^2 \right. \\ & \quad \left. + \underbrace{\frac{\hat{c}_k^2}{2} (f_{yy,n} f_n^2 + 2f_{yz,n} f_n z'_n + f_{zz,n} z_n'^2)}_{\text{second-order derivatives block}} \right]. \end{aligned} \quad (\text{B.13a})$$

Before deriving $\Delta z^{(n,m),3}$, we notice that

$$\begin{aligned} \frac{1}{6} g_{yyy,n} (\Delta y^{(n,m),1})^3 + \frac{1}{6} g_{zzz,n} (\Delta z^{(n,m),1})^3 + \frac{1}{2} g_{yyz,n} (\Delta y^{(n,m),1})^2 \Delta z^{(n,m),1} + \frac{1}{2} g_{yzz,n} \Delta y^{(n,m),1} (\Delta z^{(n,m),1})^2 = \\ \frac{1}{6} (\Delta y^{(n,m),1})^3 (g_{yyy,n} + g_{zzz,n} \mathcal{Z}_{1,n}^3 + 3g_{yyz,n} \mathcal{Z}_{1,n} + 3g_{yzz,n} \mathcal{Z}_{1,n}^2). \end{aligned}$$

Moreover,

$$\begin{aligned}\Delta z^{(n,m),1} \Delta z^{(n,m),2} &= \mathcal{Z}_{1,n} \Delta y^{(n,m),1} \left(\mathcal{Z}_{1,n} \Delta y^{(n,m),2} + \frac{1}{2} \mathcal{Z}_{2,n} (\Delta y^{(n,m),1})^2 \right) \\ \Delta y^{(n,m),1} \Delta z^{(n,m),2} &= \Delta y^{(n,m),1} \left(\mathcal{Z}_{1,n} \Delta y^{(n,m),2} + \frac{1}{2} \mathcal{Z}_{2,n} (\Delta y^{(n,m),1})^2 \right) \\ \Delta y^{(n,m),2} \Delta z^{(n,m),1} &= \mathcal{Z}_{1,n} \Delta y^{(n,m),1} \Delta y^{(n,m),2},\end{aligned}$$

so that

$$\begin{aligned}g_{yy,n} \Delta y^{(n,m),1} \Delta y^{(n,m),2} + g_{zz,n} \Delta z^{(n,m),1} \Delta z^{(n,m),2} + g_{yz,n} \Delta y^{(n,m),1} \Delta z^{(n,m),2} + g_{yz,n} \Delta y^{(n,m),2} \Delta z^{(n,m),1} = \\ \Delta y^{(n,m),1} \Delta y^{(n,m),2} (g_{yy,n} + g_{zz,n} \mathcal{Z}_{1,n}^2 + 2g_{yz,n} \mathcal{Z}_{1,n}) + \frac{1}{2} (g_{yz,n} + g_{zz,n} \mathcal{Z}_{1,n}) \mathcal{Z}_{2,n} (\Delta y^{(n,m),1})^3.\end{aligned}$$

Hence

$$\Delta z^{(n,m),3} = \mathcal{Z}_{1,n} \Delta y^{(n,m),3} + \mathcal{Z}_{2,n} \Delta y^{(n,m),1} \Delta y^{(n,m),2} + \frac{1}{6} \mathcal{Z}_{3,n} (\Delta y^{(n,m),1})^3. \quad (\text{B.14})$$

We progressively expand $\Delta z^{(n,m),3}$ in (B.14). We obtain

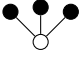
$$\begin{aligned}\Delta z^{(n,m),3} &= \mathcal{Z}_{1,n} \Delta y^{(n,m),3} + \mathcal{Z}_{2,n} \Delta y^{(n,m),1} \Delta y^{(n,m),2} \\ &\quad - g_{z,n}^{-1} \left[\Delta t^3 \frac{\hat{c}_m^3}{6} f_n^3 (g_{yyy,n} + g_{zzz,n} \mathcal{Z}_{1,n}^3 + 3g_{yyz,n} \mathcal{Z}_{1,n} + 3g_{yyz,n} \mathcal{Z}_{1,n}^2 + 3(g_{yz,n} + g_{zz,n} \mathcal{Z}_{1,n}) \mathcal{Z}_{2,n}) \right] \\ &= \mathcal{Z}_{1,n} \Delta y^{(n,m),3} + \mathcal{Z}_{2,n} \Delta t^2 \hat{c}_m f_n \sum_k \hat{a}_{mk} \left(f_{y,n} \Delta y^{(n,k),1} + f_{z,n} \Delta z^{(n,k),1} \right) \\ &\quad - g_{z,n}^{-1} \left[\Delta t^3 \frac{\hat{c}_m^3}{6} f_n^3 (g_{yyy,n} + g_{zzz,n} \mathcal{Z}_{1,n}^3 + 3g_{yyz,n} \mathcal{Z}_{1,n} + 3g_{yyz,n} \mathcal{Z}_{1,n}^2 + 3(g_{yz,n} + g_{zz,n} \mathcal{Z}_{1,n}) \mathcal{Z}_{2,n}) \right] \\ &= \mathcal{Z}_{1,n} \Delta y^{(n,m),3} + \mathcal{Z}_{2,n} \Delta t^3 \hat{c}_m f_n \sum_k \hat{a}_{mk} \hat{c}_k (f_{y,n} f_n + f_{z,n} z'_n) \\ &\quad - g_{z,n}^{-1} \left[\Delta t^3 \frac{\hat{c}_m^3}{6} f_n^3 (g_{yyy,n} + g_{zzz,n} \mathcal{Z}_{1,n}^3 + 3g_{yyz,n} \mathcal{Z}_{1,n} + 3g_{yyz,n} \mathcal{Z}_{1,n}^2 + 3(g_{yz,n} + g_{zz,n} \mathcal{Z}_{1,n}) \mathcal{Z}_{2,n}) \right] \\ &= -\Delta t^3 g_{z,n}^{-1} \left[\underbrace{\sum_k \hat{a}_{mk} \sum_j \hat{a}_{kj} \hat{c}_j g_{y,n} (f_{y,n} + f_{z,n} \mathcal{Z}_{1,n}) (f_{y,n} f_n + f_{z,n} z'_n)}_{\text{first-order derivatives block}} + \sum_k \hat{a}_{mk} \frac{\hat{c}_k^2}{2} g_{y,n} f_{z,n} \mathcal{Z}_{2,n} f_n^2 \right. \\ &\quad \left. + \sum_k \hat{a}_{mk} \frac{\hat{c}_k^2}{2} g_{y,n} (f_{yy,n} f_n^2 + 2f_{yz,n} f_n z'_n + f_{zz,n} z_n'^2) \right. \\ &\quad \left. + (g_{yy,n} + 2g_{yz,n} \mathcal{Z}_{1,n} + g_{zz,n} \mathcal{Z}_{1,n}^2) \hat{c}_m f_n \sum_k \hat{a}_{mk} \hat{c}_k (f_{y,n} f_n + f_{z,n} z'_n) \right. \\ &\quad \left. + \frac{\hat{c}_m^3}{6} f_n^3 (g_{yyy,n} + g_{zzz,n} \mathcal{Z}_{1,n}^3 + 3g_{yyz,n} \mathcal{Z}_{1,n} + 3g_{yyz,n} \mathcal{Z}_{1,n}^2 + 3(g_{yz,n} + g_{zz,n} \mathcal{Z}_{1,n}) \mathcal{Z}_{2,n}) \right] \\ &= -\Delta t^3 g_{z,n}^{-1} \left[\underbrace{\sum_k \hat{a}_{mk} \sum_j \hat{a}_{kj} \hat{c}_j g_{y,n} (f_{y,n} (f_{y,n} f_n + f_{z,n} z'_n) + f_{z,n} \mathcal{Z}_{1,n} y_n'') + \sum_k \hat{a}_{mk} \frac{\hat{c}_k^2}{2} g_{y,n} f_{z,n} \mathcal{Z}_{2,n} f_n^2}_{\text{first-order derivatives block}} \right. \\ &\quad \left. + \sum_k \hat{a}_{mk} \frac{\hat{c}_k^2}{2} g_{y,n} (f_{yy,n} f_n^2 + 2f_{yz,n} f_n z'_n + f_{zz,n} z_n'^2) \right. \\ &\quad \left. + \hat{c}_m \sum_k \hat{a}_{mk} \hat{c}_k (g_{yy,n} f_n (f_{y,n} f_n + f_{z,n} z'_n) + 2g_{yz,n} z'_n (f_{y,n} f_n + f_{z,n} z'_n) + g_{zz,n} \mathcal{Z}_{1,n}^2 f_n (f_{y,n} f_n + f_{z,n} z'_n)) \right. \\ &\quad \left. + \frac{\hat{c}_m^3}{2} g_{yz,n} \mathcal{Z}_{2,n} f_n^3 + \frac{\hat{c}_m^3}{2} g_{zz,n} \mathcal{Z}_{1,n} \mathcal{Z}_{2,n} f_n^3 \right. \\ &\quad \left. + \frac{\hat{c}_m^3}{6} (g_{yyy,n} f_n^3 + 3g_{yyz,n} f_n^2 z'_n + 3g_{yzz,n} f_n (z'_n)^2 + g_{zzz,n} (z'_n)^3) \right]. \\ &\quad \underbrace{\hspace{10em}}_{\text{third-order derivatives block}}\end{aligned}$$

Recall indeed that $z_n'' = \mathcal{Z}_{1,n}y_n'' + \mathcal{Z}_{2,n}f_n^2$ and that $z_n'z_n'' = \mathcal{Z}_{1,n}^2f_ny_n'' + \mathcal{Z}_{1,n}\mathcal{Z}_{2,n}f_n^3$. Comparing the numerical and exact expansions, we obtain the supplementary order conditions specific to order 4 reported in (4.14). An alternative, more elegant way to derive such conditions is by means of bicolour rooted trees [14, 45]. As discussed in [14], in order to distinguish derivatives with respect to y (the differential variable) and z (the algebraic variable), we need two kinds of vertices: meagre (\circ) and fat (\bullet). We associate the expression $(-g_{z,n}^{-1}g)$ with a fat vertex and f with a meagre one. Hence, the trees associated to the supplementary fourth-order conditions are

$$\begin{aligned} \sum_{l,m} b_l w_{lm} \hat{c}_m^3 &= 1, & \begin{array}{c} \bullet \\ \bullet \\ \circ \end{array} \\ \sum_{l,m,k} b_l w_{lm} \hat{c}_m \hat{a}_{mk} \hat{c}_k &= \frac{1}{2}, & \begin{array}{c} \bullet \\ \bullet \\ \circ \end{array} \\ \sum_{l,m,k} b_l w_{lm} \hat{a}_{mk} \hat{c}_k^2 &= \frac{1}{3}, & \begin{array}{c} \bullet \\ \bullet \\ \circ \end{array} \\ \sum_{l,m,k,j} b_l w_{lm} \hat{a}_{mk} \hat{a}_{kj} \hat{c}_j &= \frac{1}{6}, & \begin{array}{c} \bullet \\ \bullet \\ \bullet \\ \circ \end{array} \end{aligned}$$

The coefficients appearing in the previous relations are related to the so-called *density* of a tree τ [23, 53]. We recall that the density $\tilde{\gamma}(\tau)$ is defined recursively by

$$\tilde{\gamma}(\bullet) = 1, \quad \tilde{\gamma}(\tau) = |\tau| \prod_{i=1}^m \tilde{\gamma}(\tau_i), \quad (\text{B.15})$$

where $|\tau|$ is the *order* of the tree, i.e. the number of nodes. Here the tree τ is expressed in terms of its children, i.e. $\tau = [\tau_1, \dots, \tau_m]$, where τ_1, \dots, τ_m are the subtrees obtained by removing the root of τ . As an example, consider the tree  which has density $\tilde{\gamma}(\tau) = 4$. The coefficients appearing in the order conditions required to formally match the Taylor expansion of the exact solution are given by $1/\tilde{\gamma}(\tau)$ [53]. In the present context, however, one node plays a special role, namely the meagre node. Consequently, the coefficients reported above have to be computed by considering the tree obtained after removing the meagre root.

References

- [1] A. Abdulle. Fourth order Chebyshev methods with recurrence relation. *SIAM J. Sci. Comput.*, 23(6):2041–2054, 2002.
- [2] A. Abdulle and A.A. Medovikov. Second order Chebyshev methods based on orthogonal polynomials. *Numer. Math.*, 90(1):1–18, 2001.

- [3] A. Abdulle and G. Vilmart. PIROCK: A swiss-knife partitioned implicit-explicit orthogonal Runge–Kutta Chebyshev integrator for stiff diffusion-advection-reaction problems with or without noise. *J. Comput. Phys.*, 242:869–888, 2013.
- [4] P.F. Antonietti, S. Bonetti, M. Botti, M. Corti, I. Fumagalli, and I. Mazzieri. lymph: discontinuous poLYtopal methods for multi-physics differential problems. *ACM Trans. Math. Softw.*, 51(1):1–22, 2025.
- [5] P.F. Antonietti, F. Bonizzoni, M. Corti, and A. Dall’Olio. Discontinuous Galerkin approximations of the heterodimer model for protein-protein interaction. *Comput. Methods Appl. Mech. Engrg.*, 431:117282, 2024.
- [6] P.F. Antonietti, M. Corti, S. Gómez, and I. Perugia. A structure-preserving LDG discretization of the Fisher–Kolmogorov equation for modeling neurodegenerative diseases. *Math. Comput. Simul.*, 241:351–366, 2026.
- [7] P.F. Antonietti, S. Giani, and P. Houston. hp-version composite discontinuous Galerkin methods for elliptic problems on complicated domains. *SIAM J. Sci. Comput.*, 35(3):A1417–A1439, 2013.
- [8] P.F. Antonietti, I. Mazzieri, and F. Migliorini. A space-time discontinuous Galerkin method for the elastic wave equation. *J. Comput. Phys.*, 419:109685, 2020.
- [9] P.F. Antonietti, I. Mazzieri, A.M. Quarteroni, and F. Rapetti. Non-conforming high order approximations of the elastodynamics equation. *Comput. Methods Appl. Mech. Engrg.*, 209–212:212–238, 2012.
- [10] D.N. Arnold, F. Brezzi, B. Cockburn, and D. Marini. Unified analysis of discontinuous Galerkin methods for elliptic problems. *SIAM J. Numer. Anal.*, 39(5):1749–1779, 2001.
- [11] U.M. Ascher, S.J. Ruuth, and R.J. Spiteri. Implicit-explicit Runge–Kutta methods for time-dependent partial differential equations. *Appl. Numer. Math.*, 25(2–3):151–167, 1997.
- [12] A. Biswas, D.I. Ketcheson, S. Roberts, B. Seibold, and D. Shirokoff. Explicit Runge–Kutta methods that alleviate order reduction. *SIAM J. Numer. Anal.*, 63(4):1398–1426, 2025.
- [13] S. Boscarino. Error analysis of IMEX Runge–Kutta methods derived from differential-algebraic systems. *SIAM J. Numer. Anal.*, 45:1600–1621, 2007.
- [14] S. Boscarino. On an accurate third order implicit-explicit Runge–Kutta method for stiff problems. *Appl. Numer. Math.*, 59:1515–1528, 2009.
- [15] S. Boscarino, F. Filbet, and G. Russo. High order semi-implicit schemes for time dependent partial differential equations. *J. Sci. Comput.*, 68:975–1001, 2016.
- [16] S. Boscarino and L. Pareschi. On the asymptotic properties of IMEX Runge–Kutta schemes for hyperbolic balance laws. *J. Comput. Appl. Math.*, 316:60–73, 2017.
- [17] S. Boscarino, L. Pareschi, and G. Russo. *Implicit-explicit methods for evolutionary partial differential equations*. SIAM, 1 edition, 2024.
- [18] S. Boscarino, J. Qiu, G. Russo, and T. Xiong. High order semi-implicit WENO schemes for all-Mach full Euler system of gas dynamics. *SIAM J. Sci. Comput.*, 44:B368–B394, 2022.

- [19] S. Boscarino and G. Russo. On a class of uniformly accurate IMEX Runge–Kutta schemes and applications to hyperbolic systems with relaxation. *SIAM J. Sci. Comput.*, 31:1926–1945, 2009.
- [20] W. Boscheri, M. Tavelli, and C. Castro. An all Froude high order IMEX scheme for the shallow water equations on unstructured Voronoi meshes. *Appl. Numer. Math.*, 185:311–335, 2023.
- [21] W. Boscheri and A. Thomann. A structure-preserving semi-implicit IMEX finite volume scheme for ideal magnetohydrodynamics at all Mach and Alfvén numbers. *J. Sci. Comput.*, 100(3):67, 2024.
- [22] J. Butcher. *Numerical methods for ordinary differential equations*. Wiley, 2 edition, 2008.
- [23] J.C. Butcher. *B-series: algebraic analysis of numerical methods*, volume 55. Springer, 2021.
- [24] M. Caliari, M. Vianello, and L. Bergamaschi. The LEM exponential integrator for advection-diffusion-reaction equations. *J. Comput. Appl. Math.*, 210(1–2):56–63, 2007.
- [25] M.P. Calvo, J. De Frutos, and J. Novo. Linearly implicit Runge–Kutta methods for advection-reaction-diffusion equations. *Appl. Numer. Math.*, 37(4):535–549, 2001.
- [26] A. Cangiani, Z. Dong, E.H. Georgoulis, and P. Houston. *hp-version discontinuous Galerkin methods on polygonal and polyhedral meshes*. Springer, 2017.
- [27] A. Cangiani, E.H. Georgoulis, and P. Houston. hp-version discontinuous Galerkin methods on polygonal and polyhedral meshes. *Math. Models Methods Appl. Sci.*, 24(10):2009–2041, 2014.
- [28] M. Corti. Exploring tau protein and amyloid-beta propagation: A sensitivity analysis of mathematical models based on biological data. *Brain Multiphys.*, 7:100098, 2024.
- [29] M. Corti, F. Bonizzoni, and P.F. Antonietti. Structure preserving polytopal discontinuous Galerkin methods for the numerical modeling of neurodegenerative diseases. *J. Sci. Comput.*, 100:39, 2024.
- [30] M. Corti, F. Bonizzoni, L. Dede’, A.M. Quarteroni, and P.F. Antonietti. Discontinuous Galerkin methods for Fisher–Kolmogorov equation with application to α -synuclein spreading in Parkinson’s disease. *Comput. Methods Appl. Mech. Engrg.*, 417:116450, 2023.
- [31] P. De Luca and L. Marcellino. An IMEX scheme for a nonlinear PDE model of tumor angiogenesis. *J. Comput. Appl. Math.*, 476:117139, 2026.
- [32] M. Duarte, M. Massot, S. Descombes, C. Tenaud, T. Dumont, V. Louvet, and F. Laurent. New resolution strategy for multiscale reaction waves using time operator splitting, space adaptive multiresolution, and dedicated high order implicit/explicit time integrators. *SIAM J. Sci. Comput.*, 34(1):A76–A104, 2012.
- [33] S. Dubois, L. Gouarin, A. Hoffmann, J. Massot, M. Massot, P. Matalon, and L. Series. **samurai/ponio**: two complementary software libraries for the efficient implementation of adaptive space/time numerical schemes. In *Modeling Summer Visit*, Mountain View, CA, United States, 2025. NASA Ames Research Center. <https://hal.science/hal-05503161>.

- [34] M. Dumbser, D.S. Balsara, E.F. Toro, and C.-D. Munz. A unified framework for the construction of one-step finite volume and discontinuous Galerkin schemes on unstructured meshes. *J. Comput. Phys.*, 227(18):8209–8253, 2008.
- [35] M. Dumbser and V. Casulli. A conservative, weakly nonlinear semi-implicit finite volume scheme for the compressible Navier–Stokes equations with general equation of state. *Appl. Math. Comput.*, 272:479–497, 2016.
- [36] T. Dumont, M. Duarte, S. Descombes, M.-A. Dronne, M. Massot, and V. Louvet. Simulation of human ischemic stroke in realistic 3d geometry. *Commun. Nonlinear Sci. Numer. Simul.*, 18(6):1539–1557, 2013.
- [37] A. Ern and J.-L. Guermond. Invariant-domain preserving high-order time stepping: Ii. IMEX schemes. *SIAM J. Sci. Comput.*, 45(5):A2511–A2538, 2023.
- [38] R.A. Fisher. The wave of advance of advantageous genes. *Ann. Eugen.*, 7(4):355–369, 1937.
- [39] J.M. Franco, I. Gómez, and L. Rández. SDIRK methods for stiff ODEs with oscillating solutions. *J. Comput. Appl. Math.*, 81(2):197–209, 1997.
- [40] L. François, J. Dupays, D. Davidenko, and M. Massot. Travelling wave mathematical analysis and efficient numerical resolution for a one-dimensional model of solid propellant combustion. *Combust. Theory Model.*, 24(5):775–809, 2020.
- [41] G.J. Gassner. A skew-symmetric discontinuous Galerkin spectral element discretization and its relation to SBP-SAT finite difference methods. *SIAM J. Sci. Comput.*, 35(3):A1233–A1253, 2013.
- [42] G.J. Gassner and A.R. Winters. A novel robust strategy for discontinuous Galerkin methods in computational fluid mechanics: Why? When? What? Where? *Front. Phys.*, 8:500690, 2021.
- [43] F.X. Giraldo, J.F. Kelly, and E.M. Constantinescu. Implicit-explicit formulations of a three-dimensional nonhydrostatic unified model of the atmosphere (NUMA). *SIAM J. Sci. Comput.*, 35:1162–1194, 2013.
- [44] P. Gray and S.K. Scott. Autocatalytic reactions in the isothermal, continuous stirred tank reactor: Oscillations and instabilities in the system $a + 2b \rightarrow 3b$; $b \rightarrow c$. *Chem. Eng. Sci.*, 39(6):1087–1097, 1984.
- [45] E. Hairer and G. Wanner. *Solving ordinary differential equations II. Stiff and differential-algebraic problems*, volume 14 of *Springer Ser. Comput. Math.* Springer, 1996.
- [46] M. Han Veiga, P. Öffner, and D. Torlo. DeC and ADER: similarities, differences and a unified framework. *J. Sci. Comput.*, 87(1):2, 2021.
- [47] W. Hundsdorfer and J.G. Verwer. *Numerical solution of time-dependent advection-diffusion-reaction equations*, volume 33. Springer, 2007.
- [48] G. Izzo and Z. Jackiewicz. Highly stable implicit-explicit Runge–Kutta methods. *Appl. Numer. Math.*, 113:71–92, 2017.

- [49] C.A. Kennedy and M.H. Carpenter. Additive Runge–Kutta schemes for convection-diffusion-reaction equations. *Appl. Numer. Math.*, 44:139–181, 2003.
- [50] C.A. Kennedy and M.H. Carpenter. Diagonally implicit Runge–Kutta methods for ordinary differential equations: A review. Technical report, 2016.
- [51] C.A. Kennedy and M.H. Carpenter. Higher-order additive Runge–Kutta schemes for ordinary differential equations. *Appl. Numer. Math.*, 136:183–205, 2019.
- [52] D.I. Ketcheson, C.B. Macdonald, and S. Gottlieb. Optimal implicit strong stability preserving Runge–Kutta methods. *Appl. Numer. Math.*, 59(2):373–392, 2009.
- [53] D.I. Ketcheson and H. Ranocha. Computing with B-series. *ACM Trans. Math. Softw.*, 49(2):1–23, 2023.
- [54] A. Kvärnø. Singly diagonally implicit Runge–Kutta methods with an explicit first stage. *Numer. Math.*, 44:489–502, 2004.
- [55] C.B. Leimer Saglio, S. Pagani, M. Corti, and P.F. Antonietti. A high-order discontinuous Galerkin method for the numerical modeling of epileptic seizures. *Comput. Math. Appl.*, 205:112–131, 2026.
- [56] J. Massot, M. Massot, and L. Series. ponio, 2024. hal-04710549. <https://github.com/hpc-maths/ponio/tree/main>.
- [57] A. Meurer, C.P. Smith, M. Paprocki, O. Čertík, S.B. Kirpichev, M. Rocklin, A. Kumar, S. Ivanov, J.K. Moore, S. Singh, T. Rathnayake, S. Vig, B.E. Granger, R.P. Muller, F. Bonazzi, H. Gupta, S. Vats, F. Johansson, F. Pedregosa, M.J. Curry, A.R. Terrel, Š. Roučka, A. Saboo, I. Fernando, S. Kulal, R. Cimrman, and A. Scopatz. SymPy: symbolic computing in Python. *PeerJ Comput. Sci.*, 3:e103, 2017.
- [58] L. Micalizzi, D. Torlo, and W. Boscheri. Efficient iterative arbitrary high-order methods: An adaptive bridge between low and high order. *Commun. Appl. Math. Comput.*, 7(1):40–77, 2025.
- [59] S.P. Nørsett. C-polynomials for rational approximation to the exponential function. *Numer. Math.*, 25(1):39–56, 1975.
- [60] P. Öffner, L. Petri, and D. Torlo. Analysis for implicit and implicit-explicit ADER and DeC methods for ordinary differential equations, advection-diffusion and advection-dispersion equations. *Appl. Numer. Math.*, 212:110–134, 2025.
- [61] G. Orlando, P.F. Barbante, and L. Bonaventura. An efficient IMEX-DG solver for the compressible Navier–Stokes equations for non-ideal gases. *J. Comput. Phys.*, 471:111653, 2022.
- [62] L. Pareschi and G. Russo. Implicit-explicit Runge–Kutta schemes and applications to hyperbolic systems with relaxation. *J. Sci. Comput.*, 25:129–155, 2005.
- [63] J.E. Pearson. Complex patterns in a simple system. *Science*, 261(5118):189–192, 1993.
- [64] N. Peters. Multiscale combustion and turbulence. *Proc. Combust. Inst.*, 32(1):1–25, 2009.

- [65] T.W.H. Sheu, S.K. Wang, and R.-K. Lin. An implicit scheme for solving the convection-diffusion-reaction equation in two dimensions. *J. Comput. Phys.*, 164(1):123–142, 2000.
- [66] C. Talischi, G.H. Paulino, P. Anderson, and I.F.M. Menezes. PolyMesher: A general-purpose mesh generator for polygonal elements written in Matlab. *Struct. Multidiscip. Optim.*, 45(3):309–328, 2012.
- [67] E.F. Toro and A. Hidalgo. ADER finite volume schemes for nonlinear reaction-diffusion equations. *Appl. Numer. Math.*, 59(1):73–100, 2009.
- [68] P.J. van der Houwen and B.P. Sommeijer. Phase-lag analysis of implicit Runge–Kutta methods. *SIAM J. Numer. Anal.*, 26:214–229, 1989.
- [69] J. Weickenmeier, M. Jucker, A. Goriely, and E. Kuhl. A physics-based model explains the prion-like features of neurodegeneration in Alzheimer’s disease, Parkinson’s disease, and amyotrophic lateral sclerosis. *J. Mech. Phys. Solids*, 124:264–281, 2019.
- [70] D. Wen-Shan, Y. Hong-Juan, and S. Yu-Ren. An exact solution of Fisher equation and its stability. *Chin. Phys.*, 15(7):1414, 2006.